rial EC differentiation from Flk1-positive endothelial precursors.[28] In addition, VEGF is a known key regulator of EC differentiation from embryonic stem cells.[29] In this study, VEGFA and Notch signaling were both activated in the High group (**Figures 2A,D**). Moreover, the use of GSI clearly dissected the difference in downstream angiogenic gene expressions and in angiogenic potential between the low- and high-density cultures (**Figures 2C,E,F**). Thus, the results from this study lead to the conclusion that Notch signaling is involved in the EC differentiation of CSCs.

C-KIT positivity was markedly reduced during cultivation regardless of the plating cell-density in this study, though previous reports suggested that C-KIT positivity was preserved for several passages until transplantation.[3,7] This contrary finding between the present and the previous studies may be explained by different patient population, sampling/isolation protocols, culture protocols including plating cell-density, and/or different C-KIT detection protocols.[3,7] Although a direct relationship between C-KIT positivity and the therapeutic effects of CSCs remains unclear, plating cell-density was related to C-KIT positivity and therapeutic effects in this study, warranting further studies to investigate the significance of C-KIT expression in this treatment. In addition, the absolute number of C-KIT positive cells increased under low-density conditions compared with the high-density conditions (**Figure S1A**). Thus, low-density conditions might propagate CSCs effectively. In addition, we confirmed that CSCs expressed KDR but not Nkx2.5 (**Figure S3C**). Therefore, the characteristics of CSCs might be similar to those of cardiovascular progenitors.[12,30]

The findings of this study suggested that plating cell-density was a determinant of in vitro fundamental cellular function, including multipotency and the in vivo therapeutic effects of CSCs, and that Notch signal is one of the mechanisms responsible for this plating density-dependent function. CSCs that were cultured under High conditions showed a trend in EC differentiation with loss of SC properties such as multipotency. Although this spontaneous differentiation of CSCs was associated with activation of the Notch signaling pathway, inhibition of Notch signaling using GSI did not totally restore cellular function, including C-KIT positivity and PDT (**Figure S1B**).

One may consider several reasons for this as follows. Firstly, the Notch signal pathway was not totally inhibited by GSI treatment, though the concentration of GSI was carefully prepared by referring to a previous report[16] and doing preliminary experiments (**Figures S1C–E**). Secondly, alternative pathways to Notch signaling are present that may affect cellular properties in the maintenance culture of CSCs.[17,25,31] Finally, Notch signaling in the Low group might be slightly activated during the culture process and thus affect the properties of CSCs.

The magnitude of the therapeutic effects of CSCs in the rat AMI model was dependent upon the plating density in association with Notch signaling in this study. Although inhibition of Notch signaling in the High group did not totally restore cellular functions in vitro (**Figures 2D,3E**), functional and pathological recovery from AMI in the High group was totally restored by inhibition of Notch signaling during the course of cell preparation. This contrary finding may be explained by differences in cellular functions between in vitro and after transplantation into a rat AMI model. The cells that were transplanted into the heart were influenced by a variety of factors, such as needle injection-related mechanical damage, ischemia, inflammation or factors released from the native cardiac tissue.[32,33] These complex pathways in this treatment may yield different results for in vitro and in vivo experiments.

Regarding the therapeutic potential of CSCs, not only the cardiomyogenic potential but also differentiation potential into other lineages or just the proliferative activity of the cells might be considered. However, only a few CSC-derived vWF-positive ECs were detected (**Figure S2A**). For the SMCs, a significant difference in the percentage of $\alpha$SMA-positive cells was observed between not only the Low and High groups but also the Low and High+GSI groups (**Figure S2B**). In addition, the difference in proliferative activity in vitro might not explain the difference in therapeutic potential between the Low and High groups because the High+GSI group did not recover PDT (**Figure S1B**). Therefore, we conclude that the cardiomyogenic differentiation potential might be the main difference between the Low and High groups in terms of therapeutic potential, which was affected by Notch signaling.

In addition, we also examined the paracrine effect of transplanted CSCs and observed no significant difference in the VEGFA or HGF (**Figure 5C**) (and IGF1; **Figure S2C**) expression levels[4] among the groups (Low vs. High vs. High+GSI) at 2 days after transplantation. This was contrary to results shown in **Figures 4D,F**, which indicated that the antifibrotic effect (possibly by paracrine mechanisms) was hampered by culturing CSCs at a higher plating density. Therefore, other unknown factor(s) might be present and the "High" culture condition might hamper the expression of such protein(s) after transplantation.

This study is limited by the use of primary CSCs from mainly 1 individual patient who had idiopathic cardiomyopathy (except qPCR for C-KIT, IL-8, and VEGFA, in which 3 different patients' samples were used; **Figures 2B–D**), though a consistent fundamental difference in the cellular behavior of primary CSCs cultured with different plating densities was confirmed (PDTs with 4 different patient samples and C-KIT positivity with another patient sample; **Figures S3A,B**).

Regarding CSC preparation in the clinical scenario, the use of Notch signaling inhibitor in the culture process may be useful in enhancing the therapeutic potential of CSCs.[34] In addition, regarding the duration of the existence and localization of the transplanted cells, human-derived cardiomyocytes survived at least for 3 weeks after transplantation and resided mainly in the infarct-border zone. In this study, CSCs of human origin were transplanted into athymic nude rats. This xenotransplantation model has been used in a number of studies, which have rarely reported significant immunological reactions.[22,35] In fact, the transplanted cells in this study were not histologically involved in inflammatory reactions such as accumulation of inflammatory cells (data not shown). Thus, immune rejection in this model is minimal and does not affect the results. In addition, CSCs will be transplanted in an autologous manner in the clinical situation.[6] Therefore, the immunological reactions of this treatment may be negligible.

In conclusion, cellular properties and therapeutic potential of CSCs are affected by cell-plating density through activation of Notch signaling. Therapeutic effects of CSC-transplantation therapy for heart disease may be enhanced by reducing Notch signaling in CSCs.

## Acknowledgments

This study was financially supported by a Health Labor Sciences Research Grant from the Japanese Ministry of Health, Labor and Welfare. T.M. was supported by a Grant-in-Aid from the Japan Society for the Promotion of Science Fellows. We thank Professor Piero Anversa (Brigham and Women's Hospital, Boston, USA) and his laboratory members for technical advice. We also thank Ms Masako Yokoyama for technical instruction, Ms Atsuko Shimai and Ms Yuka Takaoka (all from Osaka University), and Ms

Noriko Kakuta (Institute of Biomedical Research and Innovation) for assistance with the manuscript.

## References


1. Roger VL, Go AS, Lloyd-Jones DM, Adams RJ, Berry JD, Brown TM, et al. Heart disease and stroke statistics: 2011 update. A report from the American Heart Association. *Circulation* 2011; **123:** e18–e209, doi:10.1161/CIR.0b013e3182009701.
2. Yamauchi T, Miyata H, Sakaguchi T, Miyagawa S, Yoshikawa Y, Takeda K, et al. Coronary artery bypass grafting in hemodialysis-dependent patients: Analysis of Japan Adult Cardiovascular Surgery Database. *Circ J* 2012; **76:** 1115–1120.
3. Bearzi C, Rota M, Hosoda T, Tillmanns J, Nascimbene A, De Angelis A, et al. Human cardiac stem cells. *Proc Natl Acad Sci USA* 2007; **104:** 14068–14073.
4. Chimenti I, Smith RR, Li TS, Gerstenblith G, Messina E, Giacomello A, et al. Relative roles of direct regeneration versus paracrine effects of human cardiosphere-derived cells transplanted into infarcted mice. *Circ Res* 2010; **106:** 971–980.
5. Choi SH, Jung SY, Kwon SM, Baek SH. Perspectives on stem cell therapy for cardiac regeneration: Advances and challenges. *Circ J* 2012; **76:** 1307–1312.
6. Bolli R, Chugh AR, D'Amario D, Loughran JH, Stoddard MF, Ikram S, et al. Cardiac stem cells in patients with ischaemic cardiomyopathy (SCIPIO): Initial results of a randomised phase 1 trial. *Lancet* 2011; **378:** 1847–1857.
7. D'Amario D, Fiorini C, Campbell PM, Goichberg P, Sanada F, Zheng H, et al. Functionally competent cardiac stem cells can be isolated from endomyocardial biopsies of patients with advanced cardiomyopathies. *Circ Res* 2011; **108:** 857–861.
8. Bartosh TJ, Wang Z, Rosales AA, Dimitrijevich SD, Roque RS. 3D-model of adult cardiac stem cells promotes cardiac differentiation and resistance to oxidative stress. *J Cell Biochem* 2008; **105:** 612–623.
9. Tang YL, Zhu W, Cheng M, Chen L, Zhang J, Sun T, et al. Hypoxic preconditioning enhances the benefit of cardiac progenitor cell therapy for treatment of myocardial infarction by inducing CXCR4 expression. *Circ Res* 2009; **104:** 1209–1216.
10. Messina E, De Angelis L, Frati G, Morrone S, Chimenti S, Fiordaliso F, et al. Isolation and expansion of adult cardiac stem cells from human and murine heart. *Circ Res* 2004; **95:** 911–921.
11. Tomita Y, Matsumura K, Wakamatsu Y, Matsuzaki Y, Shibuya I, Kawaguchi H, et al. Cardiac neural crest cells contribute to the dormant multipotent stem cell in the mammalian heart. *J Cell Biol* 2005; **170:** 1135–1146.
12. Yang L, Soonpaa MH, Adler ED, Roepke TK, Kattman SJ, Kennedy M, et al. Human cardiovascular progenitor cells develop from a KDR+ embryonic-stem-cell-derived population. *Nature* 2008; **453:** 524–528.
13. Bu L, Jiang X, Martin-Puig S, Caron L, Zhu S, Shao Y, et al. Human ISL1 heart progenitors generate diverse multipotent cardiovascular cell lineages. *Nature* 2009; **460:** 113–117.
14. Sekiya I, Larson BL, Smith JR, Pochampally R, Cui JG, Prockop DJ. Expansion of human adult stem cells from bone marrow stroma: Conditions that maximize the yields of early progenitors and evaluate their quality. *Stem Cells* 2002; **20:** 530–541.
15. Yanagisawa M, Mukai A, Shiomi K, Song SY, Hashimoto N. Community effect triggers terminal differentiation of myogenic cells derived from muscle satellite cells by quenching Smad signaling. *Exp Cell Res* 2011; **317:** 221–233.
16. Boni A, Urbanek K, Nascimbene A, Hosoda T, Zheng H, Delucchi F, et al. Notch1 regulates the fate of cardiac progenitor cells. *Proc Natl Acad Sci USA* 2008; **105:** 15529–15534.
17. Chen VC, Stull R, Joo D, Cheng X, Keller G. Notch signaling re-specifies the hemangioblast to a cardiac fate. *Nat Biotechnol* 2008; **26:** 1169–1178.
18. Kwon C, Qian L, Cheng P, Nigam V, Arnold J, Srivastava D. A regulatory pathway involving Notch1/beta-catenin/Isl1 determines cardiac progenitor cell fate. *Nat Cell Biol* 2009; **11:** 951–957.
19. Obi S, Masuda H, Shizuno T, Sato A, Yamamoto K, Ando J, et al. Fluid shear stress induces differentiation of circulating phenotype endothelial progenitor cells. *Am J Physiol Cell Physiol* 2012; **303:** C595–C606.
20. Gomes SA, Rangel EB, Premer C, Dulce RA, Cao Y, Florea V, et al. S-nitrosoglutathione reductase (GSNOR) enhances vasculogenesis by mesenchymal stem cells. *Proc Natl Acad Sci USA* 2013; **110:** 2834–2839.
21. Imanishi Y, Saito A, Komoda H, Kitagawa-Sakakida S, Miyagawa S, Kondoh H, et al. Allogenic mesenchymal stem cell transplantation has a therapeutic effect in acute myocardial infarction in rats. *J Mol Cell Cardiol* 2008; **44:** 662–671.
22. Iwasaki H, Kawamoto A, Ishikawa M, Oyamada A, Nakamori S, Nishimura H, et al. Dose-dependent contribution of CD34-positive cell transplantation to concurrent vasculogenesis and cardiomyogenesis for functional regenerative recovery after myocardial infarction. *Circulation* 2006; **113:** 1311–1325.
23. Bray SJ. Notch signalling: A simple pathway becomes complex. *Nat Rev Mol Cell Biol* 2006; **7:** 678–689.
24. Urbanek K, Cabral-da-Silva MC, Ide-Iwata N, Maestroni S, Delucchi F, Zheng H, et al. Inhibition of notch1-dependent cardiomyogenesis leads to a dilated myopathy in the neonatal heart. *Circ Res* 2010; **107:** 429–441.
25. Zakharova L, Nural-Guvener H, Gaballa MA. Cardiac explant-derived cells are regulated by Notch-modulated mesenchymal transition. *PLoS One* 2012; **7:** e37800, doi:10.1371/journal.pone.0037800.
26. Beltrami AP, Barlucchi L, Torella D, Baker M, Limana F, Chimenti S, et al. Adult cardiac stem cells are multipotent and support myocardial regeneration. *Cell* 2003; **114:** 763–776.
27. Fischer KM, Cottage CT, Wu W, Din S, Gude NA, Avitabile D, et al. Enhancement of myocardial regeneration through genetic engineering of cardiac progenitor cells expressing Pim-1 kinase. *Circulation* 2009; **120:** 2077–2087.
28. Lanner F, Sohl M, Farnebo F. Functional arterial and venous fate is determined by graded VEGF signaling and notch status during embryonic stem cell differentiation. *Arterioscler Thromb Vasc Biol* 2007; **27:** 487–493.
29. Tan KS, Tamura K, Lai MI, Veerakumarasivam A, Nakanishi Y, Ogawa M, et al. Molecular pathways governing development of vascular endothelial cells from ES/iPS Cells. *Stem Cell Rev* 2013 June 14, doi:10.1007/s12015-013-9450-7 [Epub ahead of print].
30. Bearzi C, Leri A, Lo Monaco F, Rota M, Gonzalez A, Hosoda T, et al. Identification of a coronary vascular progenitor cell in the human heart. *Proc Natl Acad Sci USA* 2009; **106:** 15885–15890.
31. Shahi P, Seethammagari MR, Valdez JM, Xin L, Spencer DM. Wnt and Notch pathways have interrelated opposing roles on prostate progenitor cell proliferation and differentiation. *Stem Cells* 2011; **29:** 678–688.
32. Segers VF, Lee RT. Stem-cell therapy for cardiac disease. *Nature* 2008; **451:** 937–942.
33. Dimmeler S, Burchfield J, Zeiher AM. Cell-based therapy of myocardial infarction. *Arterioscler Thromb Vasc Biol* 2008; **28:** 208–216.
34. Coric V, van Dyck CH, Salloway S, Andreasen N, Brody M, Richter RW, et al. Safety and tolerability of the gamma-secretase inhibitor avagacestat in a Phase 2 study of mild to moderate alzheimer disease. *Arch Neurol* 2012; **69:** 1430–1440.
35. Alshammary S, Fukushima S, Miyagawa S, Matsuda T, Nishi H, Saito A, et al. Impact of cardiac stem cell sheet transplantation on myocardial infarction. *Surg Today* 2013 March 5, doi:10.1007/s00595-013-0528-2 [Epub ahead of print].


## Supplementary Files

Supplementary File 1

Figure S1. C-KIT positive cell number, population doubling time (PDT), and qPCR analysis for cardiac stem cells under different plating densities with and without gamma secretase inhibitor (GSI).

Figure S2. Percentages of transplanted cell-derived differentiated cells in vivo and expression levels of human-specific IGF1 after transplantation.

Figure S3. Population dougling time (PDT) from 4 different patient samples, C-KIT positivity of another patient sample with different plating densities, and RT-PCR analysis for CSCs.

Please find supplementary file(s);
http://dx.doi.org/10.1253/circj.CJ-13-0534

Circulation Journal
Official Journal of the Japanese Circulation Society
http://www.j-circ.or.jp

ORIGINAL ARTICLE
Regenerative Medicine

# Myocardial Layer-Specific Effect of Myoblast Cell-Sheet Implantation Evaluated by Tissue Strain Imaging

Yasuhiro Shudo, MD; Shigeru Miyagawa, MD, PhD; Satoshi Nakatani, MD, PhD; Satsuki Fukushima, MD, PhD; Taichi Sakaguchi, MD, PhD; Atsuhiro Saito, PhD; Toshihiko Asanuma, MD, PhD; Naomasa Kawaguchi, PhD; Nariaki Matsuura, MD, PhD; Tatsuya Shimizu, MD, PhD; Teruo Okano, PhD; Yoshiki Sawa, MD, PhD

*Background:* The implantation of skeletal myoblast (SMB) cell-sheets over the damaged area of a myocardial infarction (MI) has been shown to improve global left ventricular (LV) function through a paracrine effect. However, the regeneration process has not been fully evaluated. We hypothesized that the use of tissue Doppler strain M-mode imaging to assess myocardial layer-specific strain might enable detailed visual evaluation of the regenerative ability of SMBs.

*Methods and Results:* SMBs were cultured on temperature-responsive culture dishes to generate cell-sheets. At 4 weeks after inducing anterior MI, the animals were divided into 2 groups: SMB cell-sheet implantation and sham operation (n=6 in each). A total of 30 cell-sheets ($1.5\times10^7$ cells/sheet) were placed on the epicardium, covering the infarct and border regions. Subendocardial and subepicardial strain values were measured in the infarct, border, and remote regions by tissue Doppler strain analysis. SMB cell-sheet implantation produced the following major effects: progression of LV remodeling was prevented and global LV ejection fraction increased; the subendocardial strain was significantly greater than the subepicardial strain in the treated border region; vascular density in the subendocardium was significantly higher than in the subepicardium in the treated region; the expression of vascular endothelial growth factor was significantly increased.

*Conclusions:* Tissue Doppler strain analysis allows precise evaluation of the effect of cell-sheet implantation on layer-specific myocardial function. (*Circ J* 2013; **77:** 1063–1072)

Key Words: Cytokines; Heart failure; Strain; Tissue Doppler

Heart failure still occurs frequently and is life-threatening, despite recent medical and surgical advances. Myocardial regenerative therapy is attracting growing interest as a means of improving left ventricular (LV) function in advanced heart failure.[1–3] However, recent clinical trials reported slightly disappointing results for cell transplantation by needle injection.[2–4] The major drawbacks of cell transplantation using that technique are poor retention and survival of the injected cells, local myocardial damage and potential lethal arrhythmias. The cell-sheet technique was developed to deliver cells efficiently without damaging the myocardium and, consequently, more effectively improve cardiac function than the needle injection method.[5–9] This therapeutic modality is already being used in the clinical setting.[10] It has been suggested that implantation of a skeletal myoblast (SMB) cell-sheet reverses LV remodeling via paracrine effects in which angiogenic factors constitutively released from the implanted cell-sheets induce neo-angiogenesis, increased vascular density and blood flow, thereby reversing hybernating myocardium.[5–10] However, detailed evaluation of functional improvement (eg, region-specific functional recovery associated with secreted cytokines) has not been performed. Moreover, the existing evidence base remains inconsistent, and the underlying mechanism and optimal protocols are still being debated.[11]

Tissue strain M-mode imaging based on the tissue Doppler technique (TDI-Q, Toshiba) was developed to accurately mea-

Received May 24, 2012; revised manuscript received October 15, 2012; accepted November 20, 2012; released online December 29, 2012 Time for primary review: 24 days

Department of Cardiovascular Surgery (Y. Shudo, S.M., S.F., T. Sakaguchi, A.S., Y. Sawa), Department of Health Sciences, Division of Functional Diagnostics (S.N., T.A.), Department of Pathology (N.K., N.M.), Osaka University Graduate School of Medicine, Suita; and Advanced Biomedical Engineer and Science, Tokyo Women's Medical University, Tokyo (T. Shimizu, T.O.), Japan

Presented at the American College of Cardiology's 60th Annual Scientific Session, ACCF/Herman K. Gold Young Investigator's Award in Molecular and Cellular Cardiology, New Orleans, LA, April 2–5, 2011.

Mailing address: Yoshiki Sawa, MD, PhD, Department of Cardiovascular Surgery, Osaka University Graduate School of Medicine, 2-15 Yamada-oka, Suita 565-0871, Japan. E-mail: sawa-p@surg1.med.osaka-u.ac.jp

ISSN-1346-9843 doi:10.1253/circj.CJ-12-0615

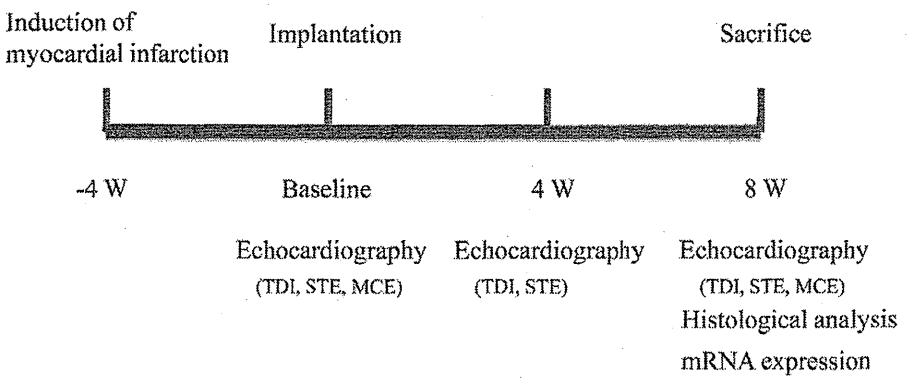


**Figure 1.** Study protocol for the assessment of cardiac function and histological analysis. TDI, tissue Doppler imaging; STE, speckle tracking echocardiography; MCE, myocardial contrast echocardiography.

sure myocardial layer-specific strain values, based on the transmural myocardial strain profile (TMSP).[12–14] Within the myocardium, the specific characteristics of each myocardial layer confer a different ability to improve regional myocardial performance.[15] We hypothesized that the myocardial layer-specific strain values might enable an assessment of regional functional improvement, based on the paracrine effects of cytokines following cell-sheet implantation. To investigate our hypothesis, we assessed the TMSP in a porcine model of myocardial infarction (MI).

## Methods

### Ethics

All studies were performed with the approval of the Ethics Committee of Osaka University. Humane animal care was used in compliance with the "Principles of Laboratory Animal Care" formulated by the National Society for Medical Research and the "Guide for the Care and Use of Laboratory Animals" prepared by the Institute of Animal Resources and published by the National Institutes of Health (Publication No 85-23, revised 1996). All authors had full access to the data and take full responsibility for its integrity. All authors have read and agreed to the manuscript as written. All procedures and evaluations, including the assessment of cardiac parameters, were carried out in a blinded manner.

### Animal Models and Study Protocol (Figure 1)

We used 20 female mini-pigs (8–10 months old, 20–25 kg; Japan Farm Co Ltd, Kagoshima, Japan). They were anesthetized with intravenous ketamine (6 mg/kg) and sodium pentobarbital (10 mg/kg) for endotracheal intubation and then maintained with inhaled sevoflurane (1–2%). The pericardial space was exposed by left thoracotomy through the 4$^{th}$ intercostal space. The distal portion of the left anterior descending coronary artery (LAD) was directly ligated, followed by placement of an ameroid constrictor around the LAD just distal of the branching of the left circumflex coronary artery (LCX) to prevent sudden cardiac death from lethal ventricular arrhythmia and intolerance of ischemia.[5,16] This technique produces an MI model that has clinical relevance and can be used for appropriate preclinical studies with minimal procedure-related mortality (6 (30%) of the 20 mini-pigs died within 48 h of surgery primarily from acute cardiac failure).

Computer-generated random allocation generated 2 randomized study groups at 1 week after the induction of MI, and autologous cells were then isolated and grown in culture for 3 weeks for implantation. At 4 weeks after MI induction, the mini-pigs were again placed under general anesthesia for echocardiography followed by either cell-sheet implantation or sham operation. Two mini-pigs in which the LV ejection fraction (LVEF) was >40%, measured by transthoracic echocardiography using the Simpson's method before the treatment, were excluded from the study. At 4 and 8 weeks after either cell-sheet implantation or sham operation, the mini-pigs were again placed under general anesthesia for echocardiography examination. The mini-pigs were killed humanely following the 8-week echocardiography study for histological and biochemical analysis of the heart tissue.

### Preparing and Grafting Skeletal Myoblast Cell Sheets

Autologous skeletal muscle weighing approximately 10–15 g was removed from the quadriceps femoris muscle, and purified autologous SMB cells were cultured for 3 weeks in preparation for implantation as described previously.[5] The cells were incubated in 60-mm temperature-responsive culture dishes (UpCell®; Cellseed, Tokyo, Japan) at 37°C for 24 h, with the cell numbers adjusted to $1.5\times10^7$ cells/dish. The dishes were then transferred to another incubator set at 20°C for 1 h to release the cultured cells as intact cell-sheets. SMB spontaneously detached to generate free-floating monolayer cell-sheets.

At 4 weeks after MI induction, the mini-pigs were randomly divided into the 2 treatment groups (n=6 in each): SMB cell-sheet implantation (Sheet group) or sham operation (Sham group). In the Sheet group, 30 cell-sheets ($1.5\times10^7$ cells/sheet) with the total cell number being $4.5\times10^8$ were implanted on the epicardium of the ischemic area (LAD region) via median sternotomy approach under general anesthesia. Cell sheets were attached and fixed to the epicardial surface by stitching around the edge of the sheet.

### Conventional Echocardiography

Global cardiac function was assessed using a commercially available echocardiograph machine with a 4.0-MHz transducer (Aplio; Toshiba, Otawara, Japan) before, and 4 and 8 weeks after cell-sheet implantation. Echocardiographic measurements included LV end-diastolic and end-systolic volumes (LVEDV

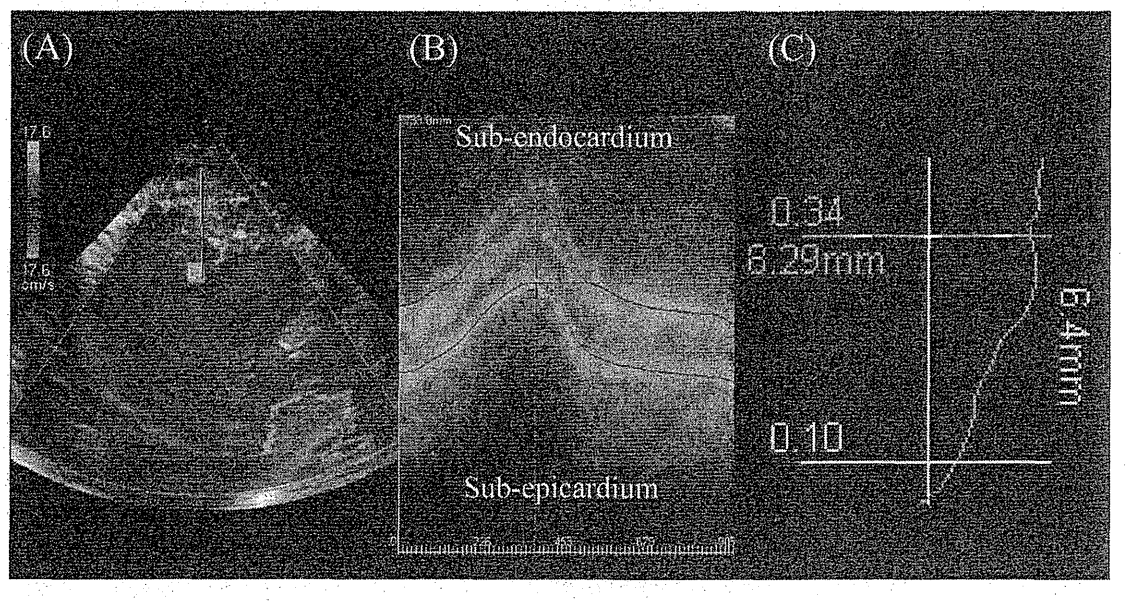


**Figure 2.** Measurement of transmural myocardial strain profile by tissue strain M-mode imaging and the indicated analysis software. (**A**) Recordings stored in the form of digital loops of 2 cardiac cycles for subsequent offline analysis. (**B**) LV endocardium and epicardium traced from an end-systolic frame. (**C**) Endocardial and epicardial borders automatically tracked through 1 cardiac cycle using analysis software (TDI-Q; Toshiba, Tokyo, Japan).

and LVESV, respectively), and LVEF, calculated as:

$$EF\,(\%) = 100 \times (LVEDV - LVESV)/(LVEDV).$$

### Myocardial Layer-Specific Strain Using Tissue Doppler Strain M-Mode Imaging

Tissue strain M-mode imaging (frame rate, 82–118 frames/s) based on the tissue Doppler technique and the corresponding analysis software (TDI-Q, Toshiba, Otawara, Japan) were used to assess myocardial layer-specific strain. Parasternal short-axis images were recorded at the level of base, mid-ventricle, and apex by tissue Doppler imaging (**Figure 2A**). To obtain a strain image, TDI-Q first calculates the myocardial displacement of all pixels of tissue by integrating myocardial velocity over a certain period. Next, strain is obtained by evaluating the change in the distance between pairs of points defined on all pixels of the image by utilizing the displacement values. The initial time frame is set at end-diastole to evaluate myocardial deformation occurring in systole. To measure local strain accurately, it is essential to accurately obtain local velocity. Therefore, the present imaging system used tissue Doppler tracking and angle-correction techniques. Tissue Doppler tracking is an automatic motion tracking technique based on tissue Doppler information. By integrating the velocity of an index point on the ventricular wall, identified from tissue Doppler imaging, we could obtain myocardial displacement and predict where the index point would move next. By repeating this procedure, the system can automatically track the motion of the index point (**Figure 2B**). With this technique, the influence of myocardial translation can be ignored. The angle-correction technique enables Doppler incident angle dependency to be partially overcome. To correct the Doppler incident angle, a contraction center is set at the center of the LV cavity at end-systole in the short-axis view. The software automatically calculates the tissue velocity toward the contraction center (V motion) by dividing the velocity toward a transducer (V beam) by the cosine of the angle ($\theta$) between the Doppler beam and the direction to the contraction center as follows:

$$V\ motion = V\ beam/\cos\theta$$

Using these 2 techniques, the software TDI-Q automatically cancelled the effect of myocardial translation and angle dependency, accurately assessing myocardial velocity, displacement, and strain. In previously described experiments, the displacement data obtained by this method correlated with true displacement.[17] Myocardial radial strain distribution over the myocardium is obtained as M-mode color-coded images and the profile of distribution (TMSP) at end-systole is shown as in **Figure 2C**. We divided the myocardium into subendocardial and subepicardial half-layers by the mid-point of the myocardium at end-systole. Mean strain values in the subendocardial half-layer and in the subepicardial half-layer were calculated by averaging the strain values over each layer in the infarcted (center of segment 13), border (edge of segment 7),[18] and remote regions (center of segment 10). In this study, the "infarcted" region was assigned predominantly to territories of the LAD, and the "remote" region was assigned to the LCX or right coronary artery.

### Histological and Immunohistochemical Analyses

At 8 weeks after the treatment, the hearts were dissected and embedded in optimum cutting temperature compound, snap-frozen in liquid nitrogen, and cut into sections. The 5-$\mu$m-thick, paraffin-embedded sections fixed in 4% paraformaldehyde were stained with hematoxylin-eosin (HE) or Masson's trichrome. Using Image J software, the infarcted area was expressed as a percentage calculated as the positively stained LV area/total LV area in sections stained with Masson's trichrome. The 5-$\mu$m thick cryosections fixed in 4% paraformaldehyde were immunofluorolabeled with anti-von Willebrand factor

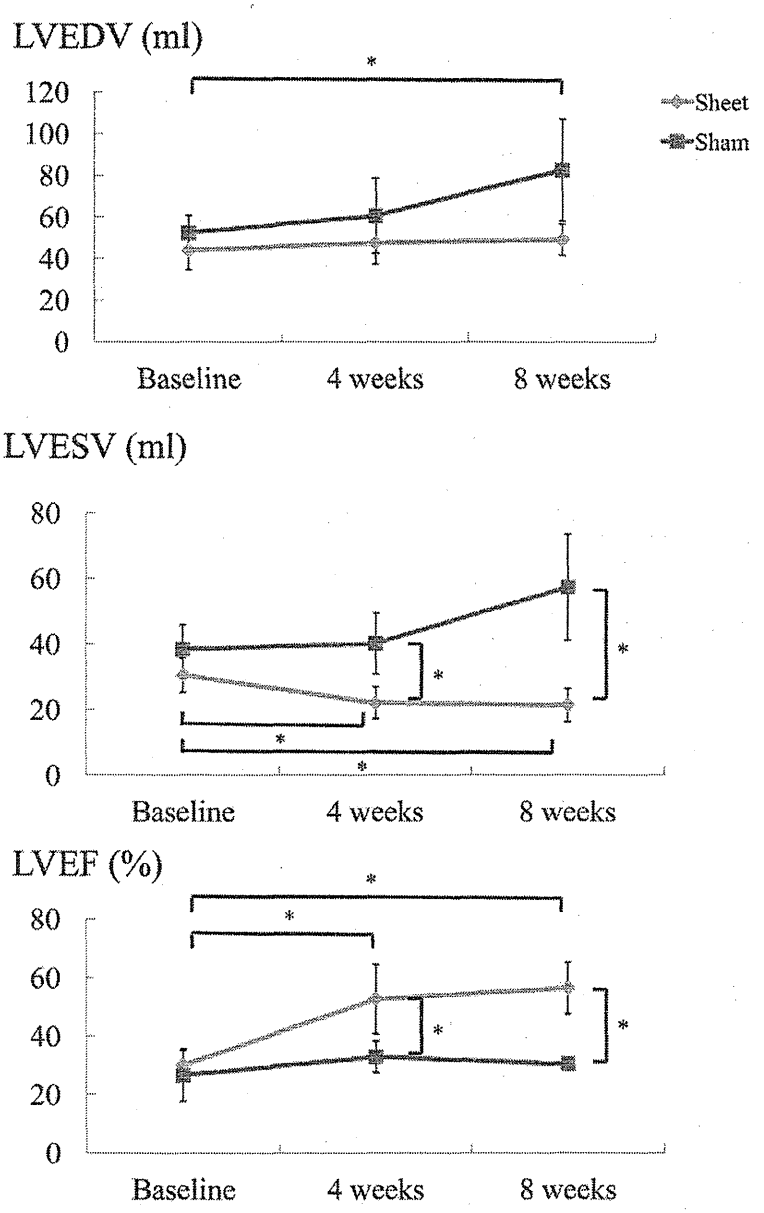


**Figure 3.** Echocardiographic analysis. LVEDV increased significantly at 8 weeks in the Sham group compared with baseline, and remained unchanged in the Sheet group. LVESV significantly decreased in the Sheet group at 4 and 8 weeks after implantation, showing a significantly lower value than that in the Sham group. LVEF significantly increased in the Sheet group at 4 and 8 weeks after implantation, showing a significantly higher value than that in the Sham group. n=6 in each group; *P<0.05. LVEDV, left ventricular end-diastolic volume; LVESV, left ventricular end-systolic volume; LVEF, left ventricular ejection fraction.

(vWF) antibody (1:250 dilution, Dako, Glostrup, Denmark). The numbers of capillary vessels that were positively stained and 5–10 $\mu$m in diameter in the subendocardium and subepicardium of the infarcted, border, and remote regions, in 10 individual, randomly selected fields per heart were counted under high-power magnification (×200) of a BioZero laser scanning microscope (Keyence, Osaka, Japan), then averaged to express vascular density (per mm$^2$).

### Analysis of mRNA Expression

Total RNA was extracted from the border region of cardiac muscle tissue and reverse transcribed into cDNA using TaqMan Reverse Transcription Reagents (Applied Biosystems, Foster City, CA, USA). Real-time polymerase chain reaction (PCR) was performed for vascular endothelial growth factor (VEGF), basic fibroblast growth factor (bFGF), brain natriuretic peptide (BNP), intercellular adhesion molecule-1, tumor necrosis factor-$\alpha$ (TNF-$\alpha$), interleukin-6 (IL-6), signal transducer and activator of transcription 3, and insulin-like growth factor-1 (IGF-1) using an ABI PRISM 7700 machine.[19] The average copy number of gene transcripts for each sample was normalized to that for GAPDH.

### Statistical Analysis

SPSS software (version 11.0, Chicago, IL, USA) was used for statistical analyses. Continuous values are expressed as the mean (standard deviation). The significance of differences was determined using a 2-tailed multiple t-test with Bonferroni correction following repeated measures analysis of variance for individual differences. P<0.05 was considered statistically significant.

## Results

### Gradual Recovery of Global Systolic LV Function

Serial changes in global systolic and diastolic LV function after cell-sheet implantation were assessed by conventional echo-

**Table. Hemodynamics and Strain Measurements**

| | SMB cell-sheet group (n=6)‡ | | | Sham operation group (n=6) | | |
|---|---|---|---|---|---|---|
| | Baseline | 4 weeks | 8 weeks | Baseline | 4 weeks | 8 weeks |
| **Heart rate (beats/min)** | 64±12 | 66±10 | 62±13 | 62±14 | 62±9 | 66±14 |
| **Blood pressure** | | | | | | |
| Systolic (mmHg) | 98±22 | 108±25 | 106±17 | 102±31 | 110±28 | 104±24 |
| Diastolic (mmHg) | 70±13 | 68±9 | 70±10 | 68±11 | 64±10 | 66±13 |
| **Conventional echocardiographic parameters** | | | | | | |
| End-diastolic volume (ml) | 44.1±9.4 | 47.7±10.2 | 49.3±7.6 | 52.5±8.3 | 60.7±18.0 | 82.7±24.5* |
| End-systolic volume (ml) | 30.6±5.3 | 22.1±4.9†,* | 21.4±5.1†,* | 38.5±7.4 | 40.2±9.3 | 57.4±16.2 |
| Ejection fraction (%) | 30.1±5.1 | 52.6±11.9†,* | 56.4±8.8†,* | 26.6±8.9 | 32.9±5.4 | 30.4±1.1 |
| **Transmural strain profile using tissue strain imaging** | | | | | | |
| Border region | | | | | | |
| Subendocardial strain (%) | 5.73±4.48 | 27.3±7.64†,* | 39.5±8.32†,* | −0.96±1.96 | −0.83±2.23 | 0.71±5.02 |
| Subepicardial strain (%) | 8.29±5.56 | 9.23±7.90 | 18.5±11.9 | 8.96±2.05 | 7.14±2.41 | 5.37±3.46 |
| Infarct region | | | | | | |
| Subendocardial strain (%) | 2.77±1.97 | 6.64±7.90 | 4.93±4.63 | −0.22±3.77 | 0.77±1.13 | −0.21±2.18 |
| Subepicardial strain (%) | −1.40±1.89 | 2.13±4.37 | 2.60±2.83 | 0.02±2.49 | 0.24±1.15 | −0.10±1.07 |
| Remote region | | | | | | |
| Subendocardial strain (%) | 67.6±17.6 | 69.2±21.6 | 75.1±14.3 | 59.0±4.36 | 51.8±7.46 | 46.8±8.29 |
| Subepicardial strain (%) | 35.5±12.3 | 43.3±17.9 | 53.8±6.91 | 38.3±8.12 | 39.9±8.28 | 35.9±5.47 |

†P<0.05 vs. Sham group, *P<0.05 vs. Baseline. ‡A total of 30 cell-sheets ($1.5\times10^7$ cells/sheet) were placed on the epicardium, covering the infarct and border regions. SMB, skeletal myoblast.

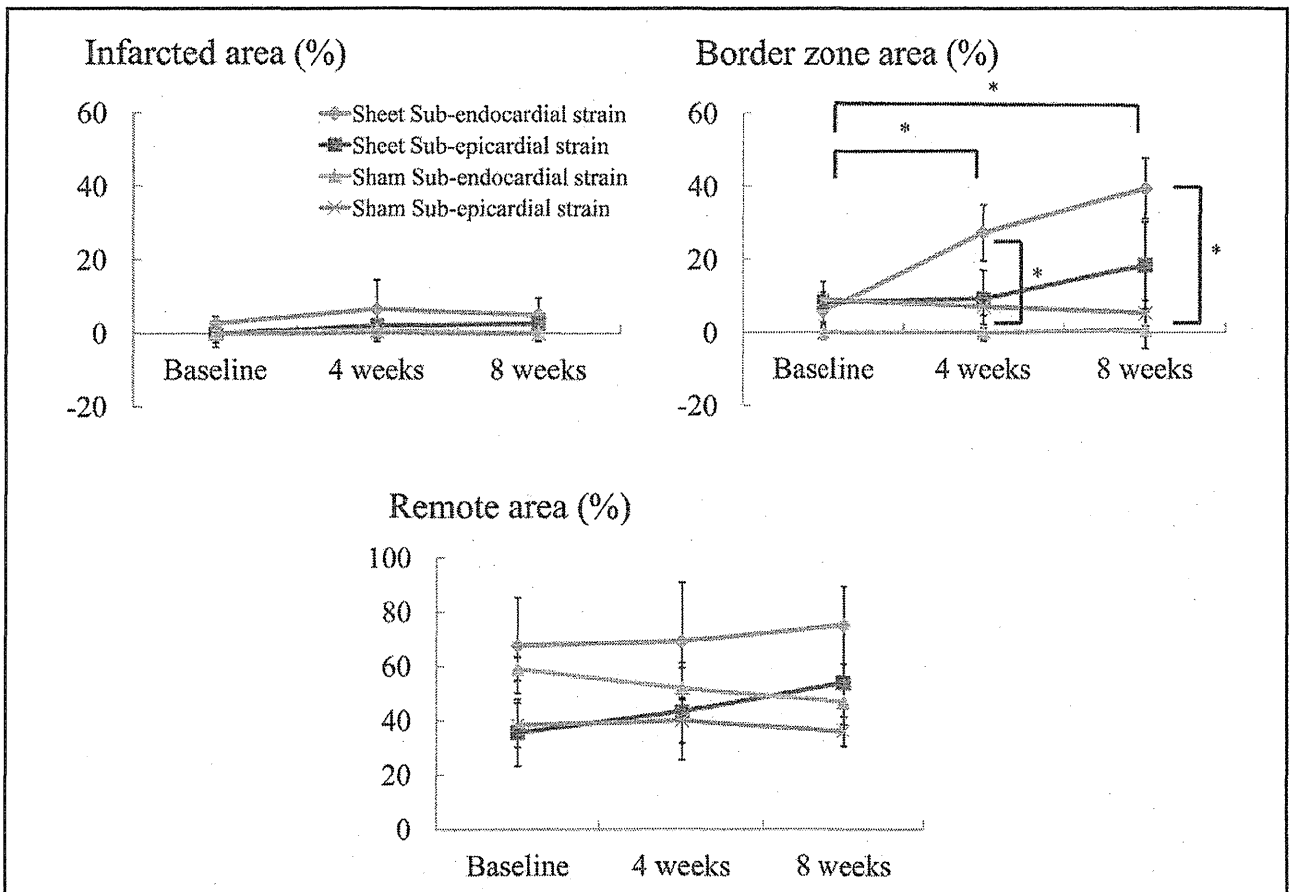


**Figure 4.** Myocardial layer strain value. In the treated border region, subendocardial strain significantly increased at 4 and 8 weeks after cell-sheet implantation, showing a significant increase in comparison with subepicardial strain. In the infarcted region, both subendocardial and subepicardial strain values were greater in the Sheet group than in the Sham group. In the remote region, no significant changes were observed. n=6 in each group; *P<0.05.

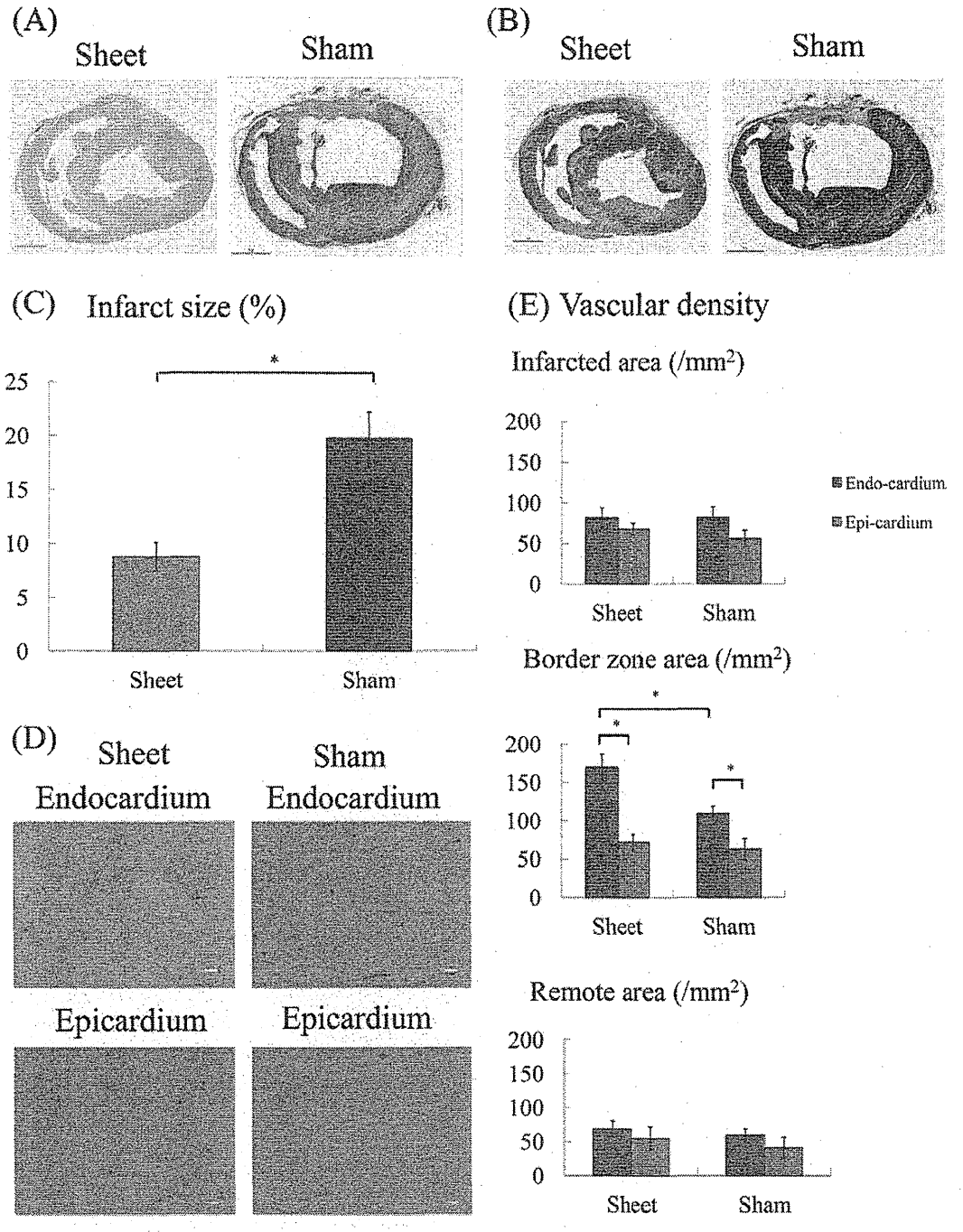


**Figure 5.** Histological findings. (**A**) Macroscopic (×40) view of the heart (HE). (**B**) Macroscopic (×40) views of the heart (Masson's trichrome). (**C**) The size of the infarcted area of the heart was significantly reduced in the Sheet group as compared with the Sham group. (**D**) Microscopic (×200) views of sections of the subendocardium and subepicardium in the treated border zone area stained with anti-von Willebrand factor (vWF) antibody (factor VIII) (bar=20 $\mu$m). (**E**) A greater number of vWF-positive blood vessels in the subendocardium compared with the subepicardium of the border zone area in the Sheet group. No significant changes are seen in the infarcted and remote areas. *P<0.05.

cardiography. Following sham operation, LVEDV and LVESV tended to increase till 8 weeks, while LVEF did not change significantly. In contrast, following SMB cell-sheet implantation, LVEDV did not change significantly, but LVESV significantly decreased and LVEF increased significantly at 4 and 8 weeks after SMB cell-sheet implantation compared with before the implantation. At 4 weeks after the treatment, LVESV was significantly smaller and LVEF was significantly greater in the Sheet group than in the Sham group, but there was no significant difference in LVEDV between them. At 8 weeks

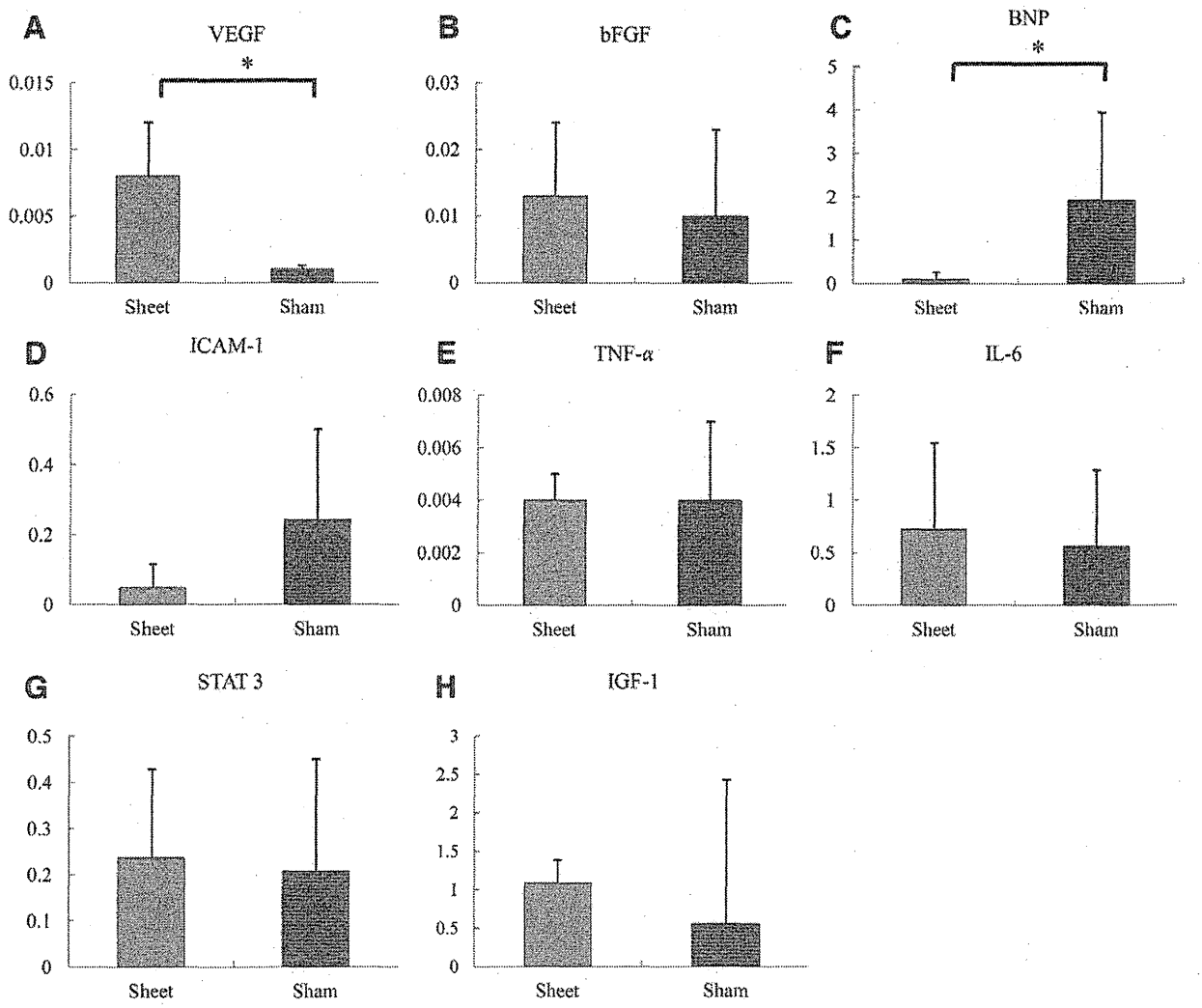


**Figure 6.** mRNA expression in cell-sheet implanted infarcted hearts determined by real-time PCR using porcine primers (A–H). VEGF mRNA expression was significantly increased in the Sheet group as compared with the Sham group. n=6 in each group; *P<0.05. PCR, polymerase chain reaction; VEGF, vascular endothelial growth factor.

after the treatment, both LVEDV and LVESV were significantly smaller and LVEF still greater in the Sheet group than in the Sham operation group (Figure 3, Table).

### Myocardial Layer-Specific Recovery

Regional LV function in the infarct, border and remote areas was also examined in a myocardial-layer specific manner to assess the regional effects of SMB cell-sheet implantation in more detail by using the TMSP at 4 and 8 weeks post cell-sheet implantation (Figure 4, Table). Before the treatment, myocardial strain values of both the subendocardium and subepicardium were significantly smaller in the infarct and border areas compared with the remote area. After the sham operation, myocardial strain in both the subendocardium and subepicardium showed similar values for the infarct, border, and remote areas for 8 weeks. In contrast, subendocardial strain significantly increased at 4 and 8 weeks after cell-sheet implantation and was significantly larger than subepicardial strain in the treated border region. In the infarcted region, both subendocardial and subepicardial strain values tended to be greater in the Sheet group than in the Sham group. In the remote region, no significant changes were observed.

### Modulation of Myocardial Structure

Myocardial structure, including fibrosis and vascularity, was assessed by HE staining, Masson's trichrome staining and immunohistochemistry for vWF at 8 weeks after the treatment (Figures 5A,B). The LV cavity was enlarged after the sham operation compared with after sheet implantation, and myocardial structure was well maintained post-sheet implantation compared with post-sham operation, as assessed by HE staining. Collagen had densely accumulated in the infarct area and was globally distributed in the remote area post-sham operation, whereas less collagen accumulated in either the infarct or remote area post-cell-sheet implantation compared with post-sham operation, as assessed by Masson's trichrome staining. The size of the infarcted area (ie, the percentage calculated as the positively stained LV area/total LV area), quantitatively

assessed by computer-based planimetry of Masson's trichrome-stained heart tissue, was significantly smaller in the Sheet group than in the Sham group (Figure 5C).

Vascular density, assessed by immunohistochemistry for vWF, in both the endocardium and epicardium, tended to be greater in the infarct and border areas than in the remote area of sham-operated hearts. In addition, vascular density in the endocardium was significantly greater than that in the epicardium in the border area post-sham operation, whereas vascular density did not differ significantly between the subendocardium and subepicardium in either the infarct or remote area of the sham-operated hearts. After cell-sheet implantation, vascular density did not differ between the subendocardium and subepicardium in either the infarct or remote area, but it was significantly greater in the subendocardium than in the subepicardium in the border region in the Sheet group. Only vascular density in the subendocardium of the border zone showed a significant difference between the sheet-implanted and sham-operated hearts (Figures 5D,E).

### Profiles of Expression of Reverse LV Remodeling-Related Molecules

A variety of molecules that are expressed intramyocardial and potentially related to reverse LV remodeling were assessed by real-time PCR. Relative expression of VEGF was significantly increased in the Sheet group compared with the Sham group, whereas other factors, such as TNF-$\alpha$, IL-6, bFGF and IGF-1, did not show any significant differences (Figure 6). Relative expression of BNP was significantly smaller post-cell-sheet implantation than post-sham operation.

## Discussion

In the present study, SMB cell-sheet implantation produced the following major effects: (1) progression of LV remodeling was prevented and global LVEF decreased; (2) subendocardial strain was significantly greater than subepicardial strain in the treated border region; (3) vascular density in the subendocardium was significantly higher than in the subepicardium of the treated region; and (4) the expression of VEGF was significantly increased. Our data therefore suggest that SMB cell-sheet implantation enhanced the paracrine effect (eg, VEGF), inducing angiogenesis and thus improving regional myocardial performance in the targeted area, and these effects were more significant in the subendocardium than in the subepicardium of the border lesion.

The mechanism of restoration of damaged myocardium by SMB cell-sheet implantation is complex and many pathways are involved in the recovery of treated myocardium.[5–7,20,21] Recent reports have described the beneficial results of SMB cell-sheet implantation in several animal experimental models and patients with heart failure, which were primarily attributed to the following factors: the secretion of cytokines from the implanted cell-sheets (ie, paracrine effect), including angiogenic growth factors, the formation of capillary networks, and finally, mechanical inhibition of LV dilatation by implantation of cell-sheets.[1,3,5–10] Previous studies supported this and have shown that SMB and bone marrow-derived mesenchymal stem cell sheets secrete growth factors (eg, VEGF) into the myocardium, and that these factors accelerate neovascularization in the damaged area.[5–10] Among the many complex molecular and cellular mechanisms, the role of VEGF and its signaling pathway has been intensively investigated in vivo.[22] Toyota et al reported that the expression of VEGF is critical to the growth of coronary collateral vessels.[23] In the present study, VEGF expression was significantly increased in the Sheet group compared with the Sham group, suggesting that SMB cell-sheet implantation induced an angiogenic response via VEGF. Although many studies have proved that released cytokines from implanted cells play a major role in generating therapeutic effects on ischemic myocardium, there is currently no modality to precisely evaluate the section of damaged myocardium affected by released cytokines.

For tissue engineering as cardiac therapy, the creation of mature and functional vessels as neo-vascularization is essential. It has been reported that capillary formation occurs via 2 basic vessel-constructing processes: angiogenesis (ie, the formation of new capillaries via sprouting or intussusception from preexisting vessels), and vasculogenesis.[24] It has been also reported that angiogenesis requires dynamic temporal and spatial regulated interaction among endothelial cells, pericytes, and angiogenic factors.[25] Together with the morphology of vessels forming within myocardial tissues, including the diameter and stability of the vessel walls, we propose another possible mechanism that vessel maturation may occur under pathological stimuli such as increased blood perfusion in the in vivo environment.

To separately elucidate the effects of SMB cell-sheet implantation on LV regional function in the treated infarcted and border areas, we used tissue Doppler derived strain and the corresponding analysis software. SMB cell-sheet implantation therapy induced an improvement in regional myocardial performance in the treated border area, but not the treated infarcted area. Moreover, we speculate that regional functional recovery may correlate well with our data for the upregulation of VEGF gene expression and significant angiogenesis in the border region of the ischemic/infarcted myocardium. In addition, on the basis of the results of an improvement in the strain value as determined by tissue Doppler derived strain, the model used in the present study can be considered as the hibernating state, especially in the border region, instead of as a model of chronic MI.[15] Taken together, the results suggest that SMB cell-sheet therapy may rescue potentially salvageable myocardium partially by reperfusion, thus improving myocardial performance. Together with the paracrine effects of the implanted SMB cell-sheet, humoral substances might have a beneficial effect on native cardiomyocytes and viable surrounding muscle cells, leading to the prevention of global myocardial remodeling.[15] Our results may support the concept of a molecular mechanism of paracrine effect associated with cardioprotective factors released following SMB cell-sheet implantation.

The TMSP showed that SMB cell-sheet implantation induced a more significant regional recovery in the subendocardium than in the subepicardium, despite the SMB cell-sheet being implanted on the epicardium. To understand this mechanism in more detail, we performed tissue strain imaging and the results reflect the fundamental differences in functional properties within the LV myocardium. Ischemic injury did not occur in a uniform manner throughout the LV myocardium. Regional differences in metabolism and energy requirements render the endocardium more vulnerable to injury. Myocardial injury and stunning therefore usually originate in the endocardium and, with time, progress to include the epicardium.[26] In general, VEGF expression is activated under hypoxic conditions, a reasonable mechanism for holding oxygen tension constant.[27] Some previous investigators suggested that a soluble VEGF receptor (ie, sVEGFR1) increases in response to hypoxia.[28,29] It seems reasonable to assume that paracrine signaling between VEGF and sVEGFR1 might be evoked predominantly

in the ischemic region to regulate angiogenesis, and improve regional myocardial performance, in the face of hypoxia. Thus, the conceptual approach of SMB cell-sheet implantation is the eliciting of a cardiac protective response (eg, angiogenesis and microcirculation) during ischemia and prevention of the progression of ischemic injury and tissue necrosis. A possible mechanism to explain our results is that SMB cell-sheet implantation induces the release of cytokines and enhances the development of microvasculature (ie, microcirculation) that might be particularly vulnerable to injury during ischemia, and upon reperfusion, enhances the recovery of myocardial performance.[30] There is currently an emerging theory that the microcirculation could be the primary target for the amelioration of the potentially devastating consequences of ischemic injury. Nevertheless, it remains to be determined whether the primary benefits of SMB cell-sheet implantation are a consequence of (1) a cardioprotective effect by contributing directly to cardiomyocyte regeneration, (2) paracrine effects emanating from the SMB cell-sheet, or (3) a combination of these effects. Also, it is unclear whether the source of the therapeutic cytokines (eg, VEGF) is the implanted cells or native cardiac cells, such as ischemic cardiomyocytes, endothelial cells, or resident macrophages.

### Study Limitations

Considerable caution must be exercised in extrapolating the present results. We did not validate myocardial strain values using other methods (eg, sonomicrometry). However, sonomicrometry is not always suitable for the assessment of transmural distribution of myocardial strain. We believe that our measurements were accurate because the displacement data obtained by our method were shown to be accurate.[31]

TDI is generally recognized as a 1D method and can measure myocardial deformation along the beam direction only. TDI-based strain estimation suffers from decorrelation caused by both axial motion and motion transverse to the beam direction. 2D speckle tracking strain imaging was introduced to overcome these limitations to myocardial imaging by estimating the 2D in-plane displacements with moderate frame rates.[32] These 2 methods are very different in principle and detail, directly affecting estimation accuracy, even of the same parameters. These differences must be noted when parameters from either method are applied clinically to myocardial contractility characterization. Moreover, the operator must avoid myocardium with large transverse motion to minimize the effect of transverse motion on TDI measurements.

Several investigators have suggested that a zone of dysfunctional myocardium caused by coronary artery occlusion might exist at the border of an infarct, with graded hypoperfusion extending out from the central region of infarction.[33,34] Subsequent reports demonstrated that coronary microvessels function essentially as end vessels with sharp boundaries between adjacent vascular beds, but that intermediate levels of mean blood flow can exist as a result of admixture of peninsulas of ischemic tissue intermingled with regions of normally perfused myocardium.[35–39] Although there is tremendous variability in the coronary artery blood supply to myocardial segments, it was believed to be appropriate to assign individual segments to specific coronary artery territories.

## Conclusions

In conclusion, assessment of the TMSP enabled precise evaluation of the effect of cell-sheet implantation on layer-specific myocardial function. Autologous SMB cell-sheet implantation enhanced the paracrine effect, induced angiogenesis, and increased blood perfusion, thus improving regional myocardial performance more effectively in the subendocardium as compared with the subepicardium of the treated border zone area.


### Sources of Funding

The present study was supported by Grants for the Research and Development of the Myocardial Regeneration Medicine Program from the New Energy Industrial Technology Development Organization (NEDO), Japan.

### Acknowledgments

We thank Mr Shigeru Matsumi and Mrs Masako Yokoyama for their excellent technical assistance.


### Disclosure

There is no conflict of interest related to this article.

### References


1. Menasche P, Hagege AA, Scorsin M, Pouzet B, Desnos M, Duboc D, et al. Myoblast transplantation in heart failure. *Lancet* 2001; **357:** 279–280.
2. Ghostine S, Carrion C, Souza LC, Richard P, Bruneval P, Vilquin JT, et al. Long-term efficacy of myoblast transplantation on regional structure and function after myocardial infarction. *Circulation* 2002; **106:** I131–I136.
3. Hagege AA, Marolleau JP, Vilqiun JT, Alheritiere A, Peyrard S, Duboc D, et al. Skeletal myoblast transplantation in ischemic heart failure: Long-term follow-up of the first phase I cohort of patients. *Circulation* 2006; **114:** I108–I113.
4. Menasche P, Hagege AA, Vilquin JT, Desnos M, Abergel E, Pouzet B, et al. Autologous skeletal myoblast transplantation for severe postinfarction left ventricular dysfunction. *J Am Coll Cardiol* 2003; **41:** 1078–1083.
5. Miyagawa S, Saito A, Sakaguchi T, Yoshikawa Y, Yamauchi T, Imanishi Y, et al. Impaired myocardium regeneration with skeletal cell sheets: A preclinical trial for tissue-engineered regeneration therapy. *Transplantation* 2010; **90:** 364–372.
6. Miyagawa S, Sawa Y, Sakakida S, Taketani S, Kondoh H, Memon IA, et al. Tissue cardiomyoplasty using bioengineered contractile cardiomyocyte sheets to repair damaged myocardium: Their integration with recipient myocardium. *Transplantation* 2005; **80:** 1586–1595.
7. Memon IA, Sawa Y, Fukushima N, Matsumiya G, Miyagawa S, Taketani S, et al. Repair of impaired myocardium by means of implantation of engineered autologous myoblast sheets. *J Thorac Cardiovasc Surg* 2009; **130:** 646–653.
8. Sekiya N, Matsumiya G, Miyagawa S, Saito A, Shimizu T, Okano T, et al. Layered implantation of myoblast sheets attenuates adverse cardiac remodeling of the infarcted heart. *J Thorac Cardiovasc Surg* 2009; **138:** 985–993.
9. Miyagawa S, Roth M, Saito A, Sawa Y, Kostin S. Tissue-engineered cardiac constructs for cardiac repair. *Ann Thorac Surg* 2011; **91:** 320–329.
10. Fujita T, Sakaguchi T, Miyagawa S, Saito A, Sekiya N, Izutani H, et al. Clinical impact of combined transplantation of autologous skeletal myoblasts and bone marrow mononuclear cells in patients with severely deteriorated ischemic cardiomyopathy. *Surg Today* 2011; **41:** 1029–1036.
11. Janseens S, Dubois C, Bogaert J, Theunissen K, Deroose C, Desmet W, et al. Autologous bone marrow-derived stem-cell transfer in patients with ST-segment elevation myocardial infarction: Double-blind, randomized controlled trial. *Lancet* 2006; **367:** 113–121.
12. Maruo T, Nakatani S, Jin Y, Uemura K, Sugimachi M, Ueda-Ishibashi H, et al. Evaluation of transmural distribution of viable muscle by myocardial strain profile and dobutamine stress echocardiography. *Am J Physiol Heart Circ Physiol* 2007; **292:** H921–H927.
13. Hasegawa T, Nakatani S, Kanzaki H, Abe H, Kitakaze M. Heterogeneous onset of myocardial relaxation in subendocardial and subepicardial layers assessed with tissue strain imaging: Comparison of normal and hypertrophied myocardium. *J Am Coll Cardiol Img* 2009; **2:** 701–708.
14. Tanimoto T, Imanishi T, Tanaka A, Yamano T, Kitabata H, Takarada S, et al. Bedside assessment of myocardial viability using transmural strain profile in patients with ST-elevation myocardial infarction: Comparison with cardiac magnetic resonance imaging. *J Am Soc Echocardiogr* 2009; **22:** 1015–1021.

15. Reimer KA, Jennings RB. The 'wavefront phenomenon' of myocardial ischemic death. II: Transmural progression of necrosis within the framework of ischemic bed size (myocardium at risk) and collateral flow. *Lab Invest* 1979; **40:** 633–644.
16. Teramoto N, Koshino K, Yokoyama I, Miyagawa S, Ose T, Zeniya T, et al. Experimental pig model of old myocardial infarction with long survival leading to chronic LV dysfunction and remodeling as evaluated by PET. *J Nucl Med* 2011; **52:** 761–768.
17. Sade LE, Severyn DA, Kanzaki H, Dohi K, Gorcsan J 3rd. Second-generation tissue Doppler with angle-corrected color-coed wall displacement for quantitative assessment of regional left ventricular function. *Am J Cardiol* 2003; **92:** 554–560.
18. Hu Q, Wang X, Lee J, Mansoor A, Liu J, Zeng L, et al. Profound bioenergetic abnormalities in peri-infarct myocardial regions. *Am J Physiol Heart Circ Physiol* 2006; **291:** H648–H657.
19. Horiguchi K, Sakakida-Kitagawa S, Sawa Y, Li ZZ, Fukushima N, Shirakura R, et al. Selective chemokine and receptor gene expressions in allografts that develop transplant vasculopathy. *J Heart Lung Transplant* 2002; **21:** 1090–1100.
20. Pagani FD, DerSimonian H, Zawadzka A, Wetzel K, Edge AS, Jacoby DB, et al. Autologous skeletal myoblasts transplanted to ischemia-damaged myocardium in humans: Histological analysis of cell survival and differentiation. *J Am Coll Cardiol* 2003; **41:** 1078–1083.
21. Suzuki K, Murtuza B, Fukushima S, Smolenski RT, Varela-Carver A, Coppen SR, et al. Targeted cell delivery into infarcted rat hearts by retrograde intracoronary infusion: Distribution, dynamics, and influence on cardiac function. *Circulation* 2004; **110:** II225–II230.
22. Toyota E, Matsunaga T, Chilian WM. Myocardial angiogenesis. *Mol Cell Biochem* 2004; **264:** 35–44.
23. Toyota E, Warltier DC, Brock T, Ritman E, Kolz C, O'Malley P, et al. Vascular endothelial growth factor is required for coronary collateral growth in the rat. *Circulation* 2005; **112:** 2108–2113.
24. Risau W. Mechanisms of angiogenesis. *Nature* 1997; **386:** 671–674.
25. Goumans MJ, Valdimarsdottir G, Itoh S, Rosendahl A, Sideras P, ten Dijke P. Balancing the activation state of the endothelium via two distinct TGF-beta type 1 receptors. *EMBO J* 2002; **21:** 1743–1753.
26. Zeng L, Hu Q, Wang X, Mansoor A, Lee J, Feygin J, et al. Bioenergetic and functional consequences of bone marrow-derived multipotent progenitor cell transplantation in hearts with postinfarction left ventricular remodeling. *Circulation* 2007; **115:** 1866–1875.
27. Shweiki D, Itin A, Soffer D, Keshet E. Vascular endothelial growth factor induced by hypoxia may mediate hypoxia-initiated angiogenesis. *Nature* 1992; **359:** 843–845.
28. Nagamatsu T, Fujii T, Kusumi M, Zou L, Yamashita T, Osuga Y, et al. Cytotrophoblasts up-regulate soluble fms-like tyrosine kinase-1 expression under reduce oxygen: An implication for the placental vascular development and the pathology of preeclampsia. *Endocrinology* 2004; **145:** 4838–4845.
29. Munaut C, Lorquet S, Pequeux C, Blacher S, Berndt S, Frankenne F, et al. Hypoxia is responsible for soluble vascular endothelial growth factor receptor-1 (VEGFR-1) but not for soluble endoglin induction in villous trophoblast. *Hum Reprod* 2008; **23:** 1407–1415.
30. Hearse DJ, Maxwell L, Saldanha C, Gravin JB. The myocardial vasculature during ischemia and reperfusion: A target for injury and protection. *J Mol Cell Cardiol* 1993; **25:** 759–800.
31. Panting JR, Gatehouse PD, Yang GZ, Grothues F, Firmin DN, Collins P, et al. Abnormal subendocardial perfusion in cardiac syndrome X detected by cardiovascular magnetic resonance imaging. *N Engl J Med* 2002; **346:** 1948–1953.
32. van Ramshorst J, Atsma DE, Beeres SL, Mollema SA, Ajmone Marsan N, Holman ER, et al. Effect of intramyocardial bone marrow cell injection of left ventricular dyssynchrony and global strain. *Heart* 2009; **95:** 119–124.
33. Buda AJ, Zotz RJ, Gallagher KP. Characterization of the functional border zone around regionally ischemic myocardium using circumferential flow-function maps. *J Am Coll Cardiol* 1986; **8:** 150–158.
34. Homans DC, Asinger R, Elsperger KJ, Erlien D, Sublette E, Mikell F, et al. Regional function and perfusion at the lateral border of ischemic myocardium. *Circulation* 1985; **71:** 1038–1047.
35. Patterson RE, Kirk ES. Analysis of coronary collateral structure, function, and ischemic border zones in pigs. *Am J Physiol Heart Circ Physiol* 1983; **244:** H23–H31.
36. Shudo Y, Matsumiya G, Takeda K, Matsue H, Taniguchi K, Sawa Y. Novel software package for quantifying local circumferential myocardial stress. *Int J Cardiol* 2011; **17:** 134–136.
37. Kainuma S, Taniguchi K, Toda K, Funatsu T, Kondoh H, Nishino M, et al. Restrictive mitral annuloplasty for functional mitral regurgitation. *Circ J* 2011; **75:** 571–579.
38. Takeda K, Matsumiya G, Hamada S, Sakaguchi T, Miyagawa S, Yamauchi T, et al. Left ventricular basal myocardial scarring detected by delayed enhancement magnetic resonance imaging predicts outcomes after surgical therapies for patients with ischemic mitral regurgitation and left ventricular dysfunction. *Circ J* 2011; **75:** 148–156.
39. Saito S, Matsumiya G, Sakaguchi T, Miyagawa S, Yoshikawa Y, Yamauchi T, et al. Risk factor analysis of long-term support with left ventricular assist system. *Circ J* 2010; **74:** 715–722.

# Spatially Oriented, Temporally Sequential Smooth Muscle Cell-Endothelial Progenitor Cell Bi-Level Cell Sheet Neovascularizes Ischemic Myocardium

Yasuhiro Shudo, MD, FAHA; Jeffrey E. Cohen, MD; John W. MacArthur, MD; Pavan Atluri, MD, FAHA; Philip F. Hsiao, BA; Elaine C. Yang, MS; Alexander S. Fairman, BA; Alen Trubelja, BS; Jay Patel, BS; Shigeru Miyagawa, MD, PhD; Yoshiki Sawa, MD, PhD; Y. Joseph Woo, MD, FAHA

***Background***—Endothelial progenitor cells (EPCs) possess robust therapeutic angiogenic potential, yet may be limited in the capacity to develop into fully mature vasculature. This problem might be exacerbated by the absence of a neovascular foundation, namely pericytes, with simple EPC injection. We hypothesized that coculturing EPCs with smooth muscle cells (SMCs), components of the surrounding vascular wall, in a cell sheet will mimic the native spatial orientation and interaction between EPCs and SMCs to create a supratherapeutic angiogenic construct in a model of ischemic cardiomyopathy.

***Methods and Results***—Primary EPCs and SMCs were isolated from Wistar rats. Confluent SMCs topped with confluent EPCs were spontaneously detached from the Upcell dish to create an SMC-EPC bi-level cell sheet. A rodent ischemic cardiomyopathy model was created by ligating the left anterior descending coronary artery. Rats were then immediately divided into 3 groups: cell-sheet transplantation (n=14), cell injection (n=12), and no treatment (n=13). Cocultured EPCs and SMCs stimulated an abundant release of multiple cytokines in vitro. Increased capillary density and improved blood perfusion in the borderzone elucidated the significant in vivo angiogenic potential of this technology. Most interestingly, however, cell fate–tracking experiments demonstrated that the cell-sheet EPCs and SMCs directly migrated into the myocardium and differentiated into elements of newly formed functional vasculature. The robust angiogenic effect of this cell sheet translated to enhanced ventricular function as demonstrated by echocardiography.

***Conclusions***—Spatially arranged EPC-SMC bi-level cell-sheet technology facilitated the natural interaction between EPCs and SMCs, thereby creating structurally mature, functional microvasculature in a rodent ischemic cardiomyopathy model, leading to improved myocardial function. (***Circulation.*** **2013;128[suppl 1]:S59–S68.)**

**Key Words:** angiogenesis ■ cardiovascular diseases ■ cells ■ endothelium ■ heart failure ■ tissue

Heart failure is the leading cause of death in the United States, with a 5-year mortality of 50%. Current treatment for heart failure entails medical optimization, along with limited revascularization and reconstructive techniques. These interventions do not address the microvascular deficiencies that develop in ischemic cardiomyopathy (ICM). Myocardial regenerative and cellular therapy is attracting growing interest as a means to improve left ventricular (LV) function in advanced heart failure. Among the many candidate cells, endothelial progenitor cells (EPCs), the precursor of blood vessels, have demonstrated excellent potential for therapeutic angiogenesis. Recent reports show beneficial effects of EPC transplantation therapy in several animal experimental models and patients with heart failure.[1–3]

The mechanism by which damaged myocardium is restored by transplanted EPCs is complex and involves many pathways. Recent large-scale clinical trials, in which EPCs were delivered using direct myocardial injection[4] or catheter-based intracoronary procedures,[5,6] reported only modest therapeutic benefits. The limited benefits are at least partially because of poor localized cell survival after transplantation, thereby greatly attenuating the angiogenic potential of EPC therapy. In addition, mature vasculature requires the presence of supporting elements, such as smooth muscle cells (SMCs), which are not delivered with simple EPC injection. In contrast, cell-sheet technology delivers cells more effectively with minimal cell dispersion and myocardial injury and improves microvascular structure, leading to better cardiac function than that attained

From the Division of Cardiovascular Surgery, Department of Surgery, University of Pennsylvania School of Medicine, Philadelphia, PA (Y.S., J.E.C., J.W.M., P.A., P.F.H., E.C.Y., A.S.F., A.T., J.P., Y.J.W.); and Department of Cardiovascular Surgery, Osaka University Graduate School of Medicine, Osaka, Japan (S.M., Y.S.).

Presented at the American Heart Association meeting in Los Angeles, CA, November 3–7, 2012.

This article was handled independently by Frank Sellke, MD, as a Guest Editor.

Correspondence to Y. Joseph Woo, MD, Division of Cardiovascular Surgery, Department of Surgery, University of Pennsylvania School of Medicine, 3400 Spruce St, 6 Silverstein, Philadelphia, PA 19104. E-mail wooy@uphs.upenn.edu



*Circulation* **is available at http://circ.ahajournals.org** **DOI: 10.1161/CIRCULATIONAHA.112.000293**

by intracoronary injection or needle injection.[7–11] Specifically, the cell-sheet technology enables the construction of a cellular system that mimics the natural architecture of a desired tissue. Here, the proposed angiogenic therapy uses the cell sheet to optimize the spatial arrangement of EPCs and SMCs to maximally induce structurally mature vasculature. The cell sheet is generated on and removed from special dishes that are grafted with a temperature-responsive polymer that changes from hydrophobic to hydrophilic when the temperature is lowered. The greatest advantage of this technique is that the cell sheet consists of densely adherent cells without requiring an artificial scaffold, it is easily manipulated and has a high ability to integrate with native tissues without destroying the cell–cell or cell–extracellular matrix (ECM) adhesions in the cell sheet.[7] In addition, we focused on the concept that the natural endothelial–pericyte spatial relationship and interaction are crucial for vessel maturation and stabilization. Thus, we hypothesized that SMCs, which are components of vascular pericytes, would enhance EPC-mediated angiogenesis and facilitate blood vessel maturation. Neoangiogenesis should yield increased blood perfusion and restoration of cardiomyocyte viability. To demonstrate clear and direct contribution of the cell-sheet EPCs and SMCs to neovasculature, we constructed multiple fate-tracking experiments. A labeled cell sheet was created with EPCs from female rats ubiquitously expressing the enhanced green fluorescent protein (GFP), along with SMCs from male rats. This cell sheet with trackable elements was then implanted in female rats.

In short, this study examined the functional benefits of transplanting the bi-level cell sheet created from cocultured EPCs and SMCs in an ICM model, compared with direct myocardial needle injection.

## Methods

### Isolation of EPCs and SMCs

Wistar rats were administered pentobarbital (100 mg/kg, IP), and then the carotid artery was dissected and transected. Bone marrow mononuclear cells were isolated from the long bones of rats by density gradient centrifugation with Histopaque 1083 (Sigma-Aldrich) and cultured in endothelial basal medium-2 supplemented with EGM-2 SingleQuot (Lonza) containing human epidermal growth factor, 5% fetal bovine serum (Sigma-Aldrich), vascular endothelial growth factor (VEGF), basic human fibroblast growth factor, recombinant human long R3 insulin-like growth factor-1, ascorbic acid, gentamicin, and amphotericin B. The combination of endothelium-specific media and the removal of nonadherent bone marrow mononuclear cells were intended to select for the EPC phenotype. EPCs were cultured for 7 days in the same medium.[2] For EPC fate tracking, we used GFP transgenic female Wistar rats.

SMCs were isolated from the thoracic aorta of wild-type male Wister rats (3 weeks old; Charles River) by primary explant technique[12] and cultured in DMEM with 20% fetal bovine serum, gentamicin, and amphotericin B to confluency for 7 days at 37°C and 5% $CO_2$. For SMC fate tracking, we used male Wistar rats.

### Bi-Level Cell-Sheet Preparation

The SMCs were plated at $1.5\times10^5$/cm$^2$ in a 35-mm Upcell dish, which is grafted with temperature-responsive polymers (CellSeed, Tokyo, Japan), and then cultured in EPC-specific medium. After 24 hours of culture at 37°C and 5% $CO_2$, EPCs were added at $1.5\times10^5$/cm$^2$ onto the Upcell dish, which was already confluent with SMCs. After 24 additional hours in culture, the dishes were transferred to another incubator, set at 20°C, for 1 hour to release the cultured cells as an intact cell sheet. Under this protocol, confluent SMCs topped with confluent EPCs were spontaneously detached from the plate as a sequentially cocultured and specifically spatially oriented SMC-EPC bi-level cell sheet (Figure 1A).[10,11]

### Production and Release of Cytokines/Chemokines

To demonstrate proangiogenic biological activity, supernatant of the cocultured cells (EPCs: $1.5\times10^5$/cm$^2$, SMCs: $1.5\times10^5$/cm$^2$), EPCs ($3.0\times10^5$/cm$^2$), or SMCs ($3.0\times10^5$/cm$^2$), after being cultured for 24 hours, was centrifuged to remove debris and contaminating cells. Levels of VEGF, hepatocyte growth factor (HGF), transforming growth factor-β (TGFβ), and stromal cell–derived factor 1α (SDF1α) in the culture supernatants were analyzed by ELISA kit (Quantikine, R&D Minneapolis, MN; n=6 in each). ELISA was performed in duplicate.

### Assessment of Cytokine Receptor Expressions by Flow Cytometry

To elucidate the biological impact of cocultured EPCs and SMCs on fetal liver kinase 1 (FLK1) and VEGF receptor 2 (VEGFR2) expression, flow cytometry was used in the EPC or SMC cultured with SMC or EPC using the transwell inserts, supplemented with recombinant VEGF, or media only for 24 hours (n=5 in each). The amount of VEGF was determined based on the results of ELISA. Test samples were incubated for 1 hour at room temperature with either mouse monoclonal anti-FLK1 (Santa Cruz Biotechnology) or rabbit anti-VEGFR2 (Abcam). After washing with cold fluorescence-activated cell sorter buffer, cells were incubated at room temperature

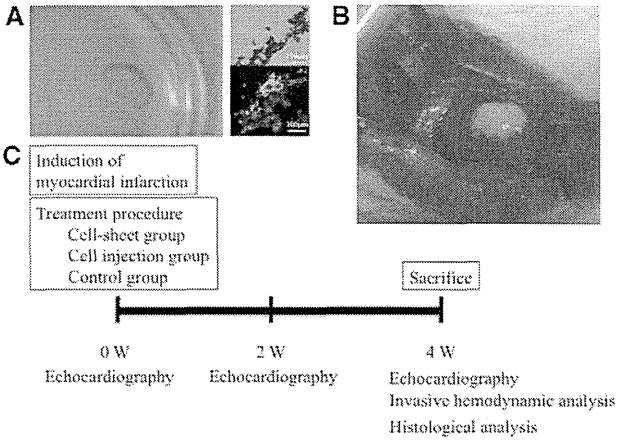


**Figure 1.** Preparation and transplantation of bi-level cocultured cell-sheet containing both endothelial progenitor cells (EPCs) and smooth muscle cells (SMCs). **A**, Confluent SMCs topped with confluent EPCs were spontaneously detached from an Upcell dish, which is grafted with temperature-responsive polymers (CellSeed, Tokyo, Japan), as a sequentially cocultured and specifically spatially oriented SMC-EPC bi-level cocultured cell-sheet. Hematoxylin-eosin staining; cross-sectional views of cell-sheet in vitro. Cocultured bi-level cell sheet maintained green fluorescent protein (GFP)-positive EPCs and Y chromosome–positive SMCs in separate layers in vitro. Red indicates rat Y chromosome; green, GFP. **B**, Bi-level cocultured cell-sheet, which consisted of $1.3\times10^6$ EPCs and $1.3\times10^6$ SMCs, was placed into the epicardium of the left ventricle covering the ischemic area. **C**, Study protocol used for assessment of cardiac function and histology. Wistar rats underwent induction of myocardial infarction by occluding the LAD permanently, followed by the concurrent treatment procedure. Cardiac function was assessed by echocardiography just before and at 2 and 4 weeks after the treatment procedure. Four weeks after the treatment procedure, invasive hemodynamic analysis and histological examination were performed after euthanasia.

for 30 minutes with Alexa 647 chicken anti-mouse IgG (Invitrogen) and Alexa 488 donkey anti-rabbit IgG (Invitrogen). The percentage of cells expressing each cell surface antigen was analyzed with a Becton Dickinson FACSCalibur flow cytometer. Data analysis was performed using FlowJo 8.8.3 (Tree Star Inc).[3,13]

## Rat ICM Model and Cell-Sheet Transplantation

Female Wistar rats (8 weeks old, 250–300g; Charles River) were anesthetized with ketamine (75 mg/kg IP) and xylazine (7.5 mg/kg IP), intubated in an endotracheal manner with a 19-gauge catheter, and mechanically ventilated (Hallowell EMC). Anesthesia was maintained by inhalation of 2.0% isoflurane (Clipper Distributing Company Llc, Saint Joseph, MO).

The proximal left anterior descending coronary artery (LAD) of Wistar rats was permanently occluded using a left thoracotomy approach. This produced a consistent and reproducible myocardial infarction encompassing 35% to 40% of the left ventricle.[1–3] Within 5 minutes after LAD ligation, the rats were allocated into 3 groups by simple randomization, considering that there were no differences among the animals at this time point: those that underwent cocultured cell-sheet transplantation (cell-sheet group, n=14), those that underwent cocultured cell injection (cell injection group, n=12), and those that underwent no intervention (control group, n=13). The rats were allowed to recover under care.

In the cell-sheet group, the cocultured bi-level cell sheet, which consists of $1.3\times10^6$ EPCs and $1.3\times10^6$ SMCs, was placed on the epicardium covering the ischemic area (Figure 1B). The cell injection group received $1.3\times10^6$ EPCs and $1.3\times10^6$ SMCs, diluted in saline for a total volume of 200 μL by direct intramyocardial injection with a 30-gauge needle. Each rat received the same number of cells. Animals were then kept in temperature-controlled individual cages for 4 weeks.

The rats were euthanized at 4 weeks after surgery by intravenous injection of 200 mg/kg of pentobarbital and 2 mEq/kg of potassium chloride, under terminal anesthesia, and the heart was excised.

## Histological and Immunohistochemical Analyses

Four weeks after treatment, the hearts were dissected and embedded in optimum cutting temperature compound for 10-μm-thick cryosections. The cryosections were used for routine hematoxylin-eosin staining to assess the myocardial structure. Masson trichrome staining was performed to assess cardiac fibrosis in the peri-infarct borderzone. The fibrotic region was calculated as the percentage of myocardial area. The data were collected from 5 individual views per heart at a magnification of ×200. The heart cryosections were also stained with an antibody to von Willebrand factor (vWF; 1:200 dilution; Abcam) to assess capillary density, which was calculated as the number of positively stained capillary vessels in 5 randomly selected fields in the peri-infarct borderzone area, per heart. The cryosections were also stained with an antibody to proliferating cell nuclear antigen (1:200 dilution; Abcam) to assess cellular proliferative activity in 5 randomly selected fields in the peri-infarct borderzone area. The cryosections were also stained with an antibody to integrin β1 (1:100 dilution; Abcam) to estimate cell–matrix attachment in 5 randomly selected fields in the peri-infarct borderzone area. Cell nuclei were counterstained with 6-diamidino-2-phenylindole (Invitrogen). The images were examined by fluorescence microscopy (Leica). Image J software was used for quantitative morphometric analysis.

## EPC-SMC Fate Tracking

The cell sheet, which consisted of EPCs from GFP transgenic female Wistar rats and SMCs from non-GFP male Wistar rats, was transplanted into the female Wistar rat heart. To detect the fate of EPCs, cryosections were stained with an anti-vWF antibody (1:1000 dilution; Abcam), anti–smooth muscle actin (SMA) antibody (1:1000 dilution; Abcam), anti–vascular endothelial-cadherin antibody (1:1000 dilution; Santa Cruz), and anti-GFP antibody (1:1000 dilution; Abcam). The secondary antibodies were Alexa Fluor 555 donkey anti-rabbit IgG (1:1000 dilution; Invitrogen) and Alexa Fluor 555 donkey anti-mouse IgG (1:1000 dilution; Invitrogen). To detect the fate of SMCs, fluorescence in situ hybridization was performed on cryosections, which were then stained with anti-SMA antibody (1:500 dilution; Abcam). The secondary antibody was Alexa Fluor 555 donkey anti-rabbit IgG (1:500 dilution; Invitrogen). Cell nuclei were counterstained with 6-diamidino-2-phenylindole. GFP-positive cells and rat Y chromosome–positive cells were counted, respectively, and corrected by total number of tissue cells to estimate the survival cells quantitatively. GFP- and vWF-positive cells were counted and corrected by total number of GFP-positive cells to examine vascular regeneration. Rat Y chromosome– and SMA-positive cells were counted and corrected by total number of rat Y chromosome–positive cells to examine vascular regeneration.

## Myocardial Perfusion Analysis

To quantify myocardial perfusion, at 4 weeks after treatment 200 μg of fluorescein-labeled *Lycopersicon esculentum* (tomato) lectin (Vector Laboratories) was injected into the supradiaphragmatic inferior vena cava and allowed to circulate for 10 minutes. After lectin perfusion, the hearts were explanted and snap-frozen in liquid nitrogen. One-hundred twenty sequential images were obtained through 100-μm thick myocardial sections at the level of the papillary muscle using scanning laser confocal microscopy (z-series, ×20 air magnification, Zeiss LSM-510 Meta Confocal Microscope). Three-dimensional reconstructions of the image stacks were created using Velocity Software v.3.61 (Improvision). Fluorescein-labeled voxels were quantified as a percentage of total tissue section voxels, creating a quantifiable measurement of perfusion per unit of myocardial tissue volume.[2,3]

## Echocardiographic Assessment

Echocardiography was performed under general anesthesia using 1.0% inhaled isoflurane just before and at 2 and 4 weeks after the treatment procedure (SONOS 7500, Philips Medical Systems, Andover, MA) with a 12-MHz transducer at an image depth of 2 cm (cell sheet, n=7; cell injection, n=8; control, n=9; Figure 1C). LV end-diastolic diameter (LVEDD), LV end-systolic diameter (LVESD), and end-diastolic anterior wall thickness at the level of the papillary muscles were measured for ≥3 consecutive cardiac cycles following the American Society for Echocardiology leading-edge method. Fractional shortening (FS) and ejection fraction (EF) were calculated as parameters of systolic function.[2,3,8] All analyses were performed by a single investigator in a group-blinded fashion.

## Invasive Hemodynamic Assessment

Four weeks after the treatment procedure, animals (cell-sheet, n=6; cell injection, n=6; control, n=8) underwent invasive hemodynamic measurements with a pressure–volume conductance catheter (SPR-869; Millar Instruments, Inc; Figure 1C). The catheter was calibrated via 5-point cuvette linear interpolation with parallel conductance subtraction by the hypertonic saline method.[2,3] Rats were anesthetized using 1.0% inhaled isoflurane, and the catheter was introduced into the LV with a closed-chest approach via the right carotid artery. Measurements were obtained before and during inferior vena cava occlusion to produce static and dynamic pressure–volume loops under varying load conditions. Data were recorded and analyzed with LabChart version 6 software (AD Instruments) and ARIA Pressure Volume Analysis software (Millar Instruments, Inc). After hemodynamic assessment, the heart was removed for further histological analyses.

## Statistical Analysis

Continuous variables are expressed as mean±SE. Comparisons between 2 groups were made using the Wilcoxon–Mann–Whitney *U* test because of small sample sizes. For comparisons among 3 groups, we used the Kruskal–Wallis test, followed by the post hoc pairwise Wilcoxon–Mann–Whitney *U* test. The multiplicity in pairwise comparisons was corrected by the Bonferroni procedure. A $P<0.05$ was

considered statistically significant. All statistical calculations were performed using SPSS software (version 11.0; SPSS Inc, Chicago, IL) and JMP 9.0 (SAS Institute Inc, Cary, NC).

### Animal Care and Biosafety

Wistar rats were obtained from Charles River. Food and water were provided ad libitum. This investigation conforms with the Guide for the Care and Use of Laboratory Animals published by the US National Institutes of Health (NIH Publication No. 85-23, revised 1996) and was approved by the Institutional Animal Care and Use Committee of the University of Pennsylvania (protocol 803394).

## Results

### Production and Release of Cytokines/Chemokines by Coculturing EPC With SMC

VEGF was significantly higher in the coculture supernatant than the SMC-only group and tended to be higher than the EPC-only group (Figure 2A). The secretion of HGF was remarkably enhanced in the coculture supernatant, whereas HGF levels were not evident in either the EPC- or SMC-alone group (Figure 2B). The concentration of TGFβ was significantly higher in the coculture supernatant than both the EPC- and SMC-only groups (Figure 2C). The secretion of SDF1α was remarkably higher in the cocultured group compared with EPC and SMC alone (Figure 2D).

### Upregulated Expressions of FLK1 and VEGFR2 on Either EPC or SMC Under Cytokines-Rich Medium of SMC or EPC

Flow cytometric analysis demonstrated that the percentage of FLK1$^+$ EPCs and VEGFR2$^+$ EPCs in total EPC population was 1.3±0.3% and 3.2±0.8%, respectively. Supplementation with VEGF significantly increased the percentage of FLK1$^+$ EPCs (17.2±3.2%) and VEGFR2$^+$ EPCs (32.0±5.4%). Furthermore, the percentage of FLK1$^+$ and VEGFR2$^+$ EPCs was significantly greater after coculturing with SMC (FLK1$^+$, 39.6±9.2%; VEGFR2$^+$, 52.5±9.8%; Figure 3A and 3B).

Flow cytometric analysis demonstrated a statistically significant increase in the percentage of FLK1$^+$ SMCs cocultured with EPC compared with SMC alone (75.7±5.4 versus 23.9±2.5%; $P$=0.02). Addition of VEGF significantly increased FLK1$^+$ SMCs compared with SMC (Figure 3C and 3D). There was no significant difference in the VEGFR2$^+$ expression on SMCs ($P$=0.14, Kruskal–Wallis test).

### Enhanced Capillary Density and Microvascular Perfusion After Cocultured Cell-Sheet Transplantation

A large number of vWF-positive blood vessels were detected in the peri-infarct borderzone myocardium after cell-sheet therapy compared with injection alone (Figure 4A). This demonstrated a superior enhancement of capillary density in the cell-sheet group (Figure 4B).

Similarly, lectin microangiography of the peri-infarct borderzone myocardium sections revealed a more densely and well-developed capillary network in the cell-sheet group compared with injection alone (Figure 4C). Quantitative analysis showed significantly enhanced perfusion in the peri-infarct borderzone myocardium in the cell-sheet group (Figure 4D).

### Enhanced Cell Proliferation Activity After Cocultured Cell-Sheet Transplantation

A large number of proliferating cell nuclear antigen-positive cells were identified in the peri-infarct borderzone myocardium after cell-sheet therapy compared with control (Figure 4E and 4F).

### Migration of EPCs and SMCs to Myocardium Contributing to Neovasculature

Cocultured bi-level cell sheet contained GFP-positive EPCs and Y chromosome–positive SMCs in separate layers in vitro (Figure 1A).

Four weeks after transplantation, the GFP-positive EPCs were detected in the myocardium at the transplanted site at an appropriate depth of 650 μm (Figure 4G). Immunostaining for vWF and GFP showed that transplanted EPCs were able to contribute to neovascularization of the host myocardium (Figure 4H). This was further supported by immunostaining for vascular endothelial-cadherin and GFP (Figure 4I). In addition, staining with antibody to SMA and GFP indicated that GFP-positive EPCs originating from the transplanted cocultured bi-level cell sheet migrated into the engineered

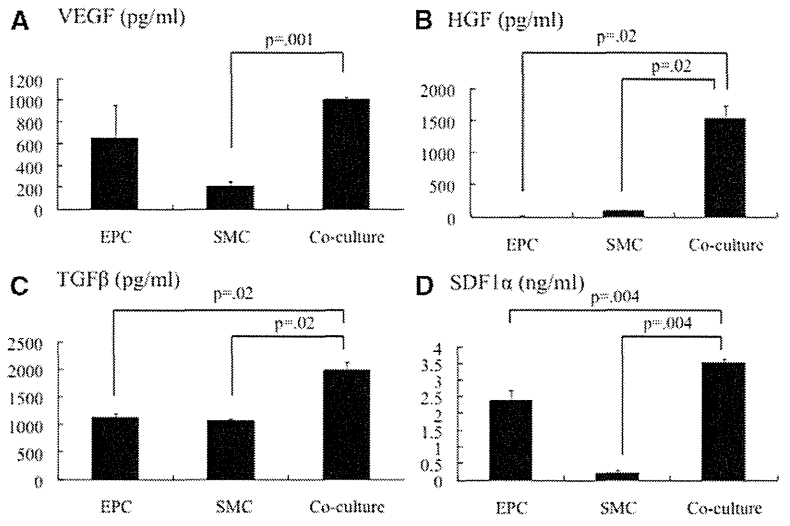


**Figure 2. A**, Vascular endothelial growth factor (VEGF), (**B**) hepatocyte growth factor (HGF), (**C**) transforming growth factor-β (TGFβ), and (**D**) stromal cell–derived factor 1α (SDF1α) in the culture supernatant, measured by ELISA. Cocultured endothelial progenitor cells (EPCs) with smooth muscle cells (SMCs) secreted abundant VEGF, HGF, TGFβ, and SDF1α compared with either EPC or SMC (n=6 in each; VEGF, $P$=0.002; HGF, $P$=0.01; TGFβ, $P$=0.01; SDF1α, $P$=0.001; Kruskal–Wallis test).

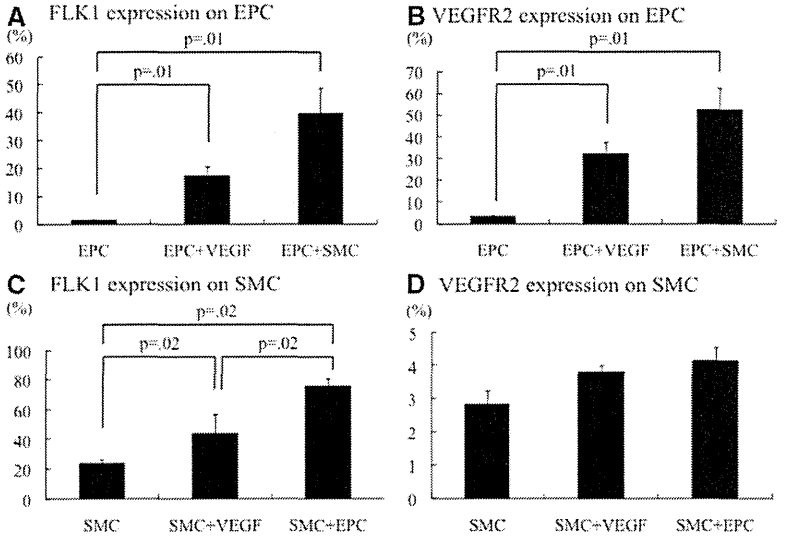


**Figure 3.** To elucidate the biological impact of cocultured endothelial progenitor cell (EPC)-smooth muscle cells (SMCs) on FLK1 and vascular endothelial growth factor receptor 2 (VEGFR2) expression, flow cytometry was used to study both EPC and SMC expression of these markers in the following settings: cocultured, cultured with VEGF, and cultured alone. The amount of VEGF used was determined based on the results of ELISA. **A** and **B**, The percentage of FLK1$^+$ EPC and VEGFR2$^+$ EPC was greatest in a cocultured setting (n=5 in each; FLK1 expression on EPC, $P$=0.01; VEGFR2 expression on EPC, $P$=0.01; Kruskal–Wallis test). **C** and **D**, Analysis of SMC FLK1$^+$ expression demonstrated a significant increase in the cocultured group. There was no significant difference in the VEGFR2$^+$ expression on SMC (n=4 in each; FLK1 expression on SMC, $P$=0.01; VEGFR2 expression on SMC, $P$=0.14; Kruskal–Wallis test).

myocardial tissues and were circumferentially surrounded by SMA-positive tissues (Figure 4J). Finally, to track SMCs from the cell sheet, we performed fluorescence in situ hybridization immediately to identify male SMCs in the female recipient. After the cell-sheet transplantation, GFP-positive EPCs and Y chromosome–positive SMCs were detected with a thickness of ≈50 μm into the epicardium (Figure 4K). Rat Y chromosome SMCs were partially able to differentiate into SMA-positive tissues (Figure 4L). Quantitative analysis showed a greater percentage of GFP-positive cells and rat Y chromosome–positive cells, respectively, in the cell-sheet group compared with cell injection (Figure 4M). Quantitative analysis of vascular regeneration showed that the number of both GFP- and vWF-positive cells is 18±3/hpf (60% of GFP-positive cells), which participated in new blood vessel formation. In addition, the number of both Y chromosome– and SMA-positive cells is 7±2/hpf (45% of rat Y chromosome cells), which participated in new blood vessel formation. One week after treatment, a large number of integrin β1–positive cells were observed in the peri-infarct borderzone myocardium after cell-sheet therapy compared with cell injection and control (Figure 4N and 4O).

### LV Remodeling After Cell-Sheet Transplantation

The LV myocardial structure was superiorly maintained after cell-sheet transplantation compared with cell injection and control, as assessed by hematoxylin-eosin staining (Figure 5A). In addition, cell-sheet therapy significantly attenuated collagen accumulation in the infarct area compared with cell injection and control, as demonstrated by Masson trichrome staining (Figure 5B and 5C).

### Cardiac Functional Recovery After Cell-Sheet Transplantation

The effects of cocultured bi-level cell-sheet transplantation on cardiac function were assessed in a rat ICM model. After permanent occlusion of the LAD, EF, FS, and anterior wall thickness (baseline, 1.7±0.1 mm; at 2 weeks, 0.8±0.1 mm, at 4 weeks, 0.8±0.1 mm; $P$=0.0001, Kruskal–Wallis test) showed steady reductions, whereas EDD/ESD showed steady increases (EDD, $P$=0.0002; ESD, $P$=0.0001; Kruskal–Wallis test), suggesting progressive LV remodeling. After cocultured cell injection, the heart showed mild recovery, including increases in FS and EF. At 4 weeks after treatment, EF and FS tended to be greater after cocultured cell injection than the control; however, an even greater recovery was observed after cell-sheet transplantation (Figure 6A and 6B). At 4 weeks, the bi-level cell-sheet group had a significantly greater EF and FS and significantly improved EDD and ESD compared with either cell injection or control (Figure 6C and 6D).

Assessment by pressure–volume catheter further confirmed the cell-sheet–induced functional enhancement demonstrated by the echocardiographic data. Four weeks after transplantation, the maximal rate of change in LV pressure (max. $dP/dt$) and end-systolic pressure–volume relationship were significantly enhanced in the cell-sheet group compared with cell injection and control (Figure 7). Mimimal rate of change in LV pressure (min. $dP/dt$) and cardiac output were higher in the cell-sheet group than the other 2 groups, but the difference was not significant.

## Discussion

This study revealed a multifaceted mechanism by which the targeted implantation of an EPC-SMC bi-level cell-sheet enhances myocardial function in a rodent model of ICM. A significant chemokine effect was observed in vitro where cocultured EPC-SMCs stimulated an abundant release of SDF1α, VEGF, HGF, and TGFβ; this effect is a mechanistic component of the augmented angiogenesis demonstrated in vivo. More importantly, however, the data clearly established direct migration of the cell-sheet EPCs and SMCs into the myocardium and confirmed these cells to be some elements of newly formed functional vasculature. The observed increased capillary density and improved blood perfusion in the borderzone elucidated the significant in vivo angiogenic potential of this technology. Furthermore, cell fate–tracking experiments strongly suggested the cell-sheet EPCs and SMCs as components of newly assembled vasculature. With regard to cell engraftment, the cell-sheet group performed superiorly, demonstrating improved cell–matrix attachment compared

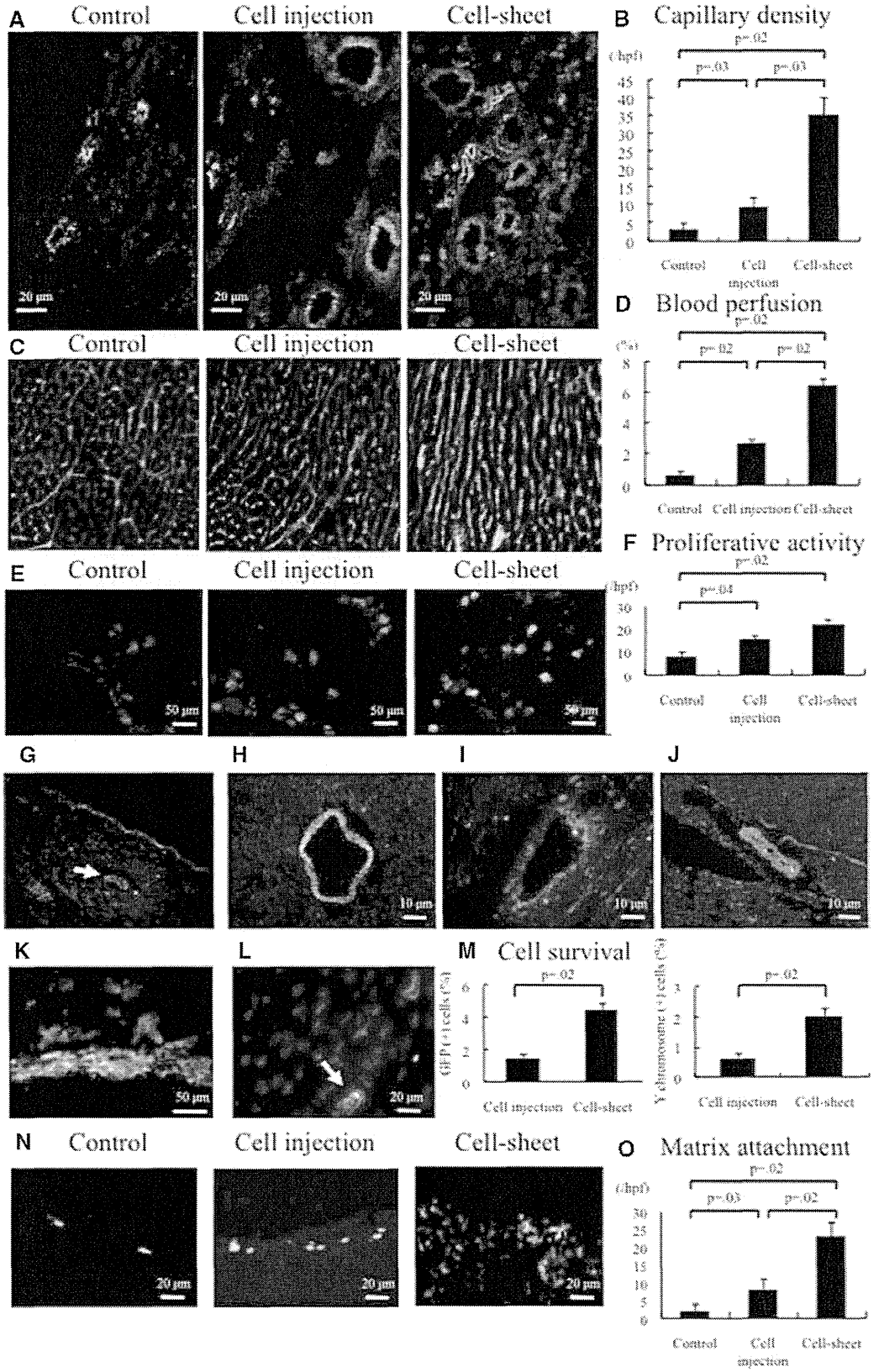


**Figure 4.** Effects on left ventricular remodeling, capillary density, and microvascular perfusion by bi-level cocultured cell-sheet transplantation (cell-sheet), cocultured cell injection (cell injection), and control (control) 4 weeks after the treatment procedure. **A**, Representative von Willebrand factor (vWF) staining of the borderzone myocardium. **B**, Quantification of capillary density. Capillary density was significantly enhanced in the cell-sheet groups compared with other groups (cell-sheet, n=4; cell injection, n=3; control, n=4; *P*=0.01, Kruskal–Wallis test). **C**, Representative lectin microangiographic imaging from the borderzone myocardium (×20 magnification). **D**, Quantitative analysis showed enhanced blood perfusion in the cell-sheet group compared with the other groups (cell sheet, n=4; cell injection, n=4; control, n=4; *P*=0.01, Kruskal–Wallis test). **E**, Representative antiproliferative cell nuclear

(*Continued*)

**Figure 4. Continued** antigen staining of the borderzone myocardium. **F**, Quantification of cell proliferative activity. Proliferative activity was significantly enhanced in the cell-sheet group compared with control (cell sheet, n=4; cell injection, n=4; control, n=4; *P*=0.02, Kruskal–Wallis test). **G**, Immunoconfocal microscopy demonstrated abundant green fluorescent protein (GFP)-positive cells in the myocardium. **H**, Cryosections were stained with an antibody to vWF and GFP to detect the fate of endothelial progenitor cells (EPCs) in the heart. Immunostaining for vWF and GFP showed that transplanted EPCs over the borderzone myocardium were able to contribute directly to neovascularization of the host myocardium. Green indicates GFP; red, vWF; blue, nuclei. **I**, Immunostaining for vascular endothelial (VE)-cadherin and GFP showed that transplanted EPCs were able to contribute to neovascularization of the host myocardium. Green indicates GFP; red, VE-cadherin; blue, nuclei. **J**, In addition, staining with antibody to smooth muscle actin (SMA) and GFP demonstrated that GFP-positive EPCs originating from the transplanted cocultured bi-level cell sheet migrated into the treated myocardial tissues and were circumferentially supported by SMA-positive tissues. Green indicates GFP; red, SMA; blue, nuclei. **K**, Furthermore, to track SMCs from the cell sheet, we performed fluorescence in situ hybridization to identify male SMCs in the female recipient. Immediately after the cell-sheet transplantation, GFP-positive EPCs and Y chromosome–positive SMCs were detected in the epicardium. Red indicates rat Y chromosome; green, GFP. **L**, Rat Y chromosome SMCs were able to differentiate into SMA-positive tissues (white arrow). Red indicates SMA; yellow, rat Y chromosome; blue, nuclei. **M**, Quantitative analysis of cell survival estimation. GFP-positive cells and rat Y chromosome–positive cells were counted, respectively, and corrected by total number of tissue cells to examine the survival cells quantitatively. **N**, Representative anti-integrin β1 staining of the borderzone myocardium. **O**, Quantification of cell–matrix attachment. Cell–matrix attachment was significantly enhanced in the cell-sheet group compared with the other groups (cell sheet, n=4; cell injection, n=4; control, n=4; *P*=0.01, Kruskal–Wallis test).

with injection alone. The robust angiogenic effect of bi-level cell-sheet translated to enhanced myocardial function of the ischemic heart.

Our group has investigated the effects of EPCs as a neovasculogenic therapy for ICM using EPC therapy alone,[14] with seeded EPCs,[13] and with a tissue-engineered matrix.[2] Based on these findings, we began to explore the effects of ex vivo expanded EPCs. Systemic and direct myocardial injection of EPCs, however, is fraught with complications, such as cell dispersion and high percentages of cell loss. In this study, we used cell-sheet technology, which allows efficient delivery of cells onto the ischemic area of myocardium with minimal myocardial injury and cell dispersion, preserves cell–cell and cell–ECM architectural structure, and might, therefore, be more applicable to human translation.[15]

Given our previous work and experience with cell-sheet technology, one possible mechanism is likely to include cytokine release and hematopoietic stem cell recruitment.[7–9] Previous studies have shown that EPCs acted as the natural supplier of SDF1α,[16] VEGF,[17] HGF,[18] and TGFβ.[19] Their roles and signaling pathways have been intensively investigated; SDF1α is related to cell migration, proliferation, and migration[2,13,16]; VEGF is critical to stimulate endothelial cell proliferation and migration to initiate neovascularization[19]; HGF is beneficial to an impaired heart and is associated with an antifibrotic effect.[7,20] Together with our findings, it is reasonable to conclude that coculturing EPCs with SMCs enhanced the secretion of cytokines, such as SDF1α, VEGF, HGF, and TGFβ, compared with either EPCs or SMCs, thus leading to the enhanced proliferation of cardiomyocytes and stimulation of angiogenesis. To understand the detailed mechanism by which coculturing enhances cytokine secretion, we performed additional investigations from a new perspective. We found that FLK1 and VEGFR2 were upregulated by additional VEGF, which were even more enhanced by numerous cytokines containing cell-culturing medium, suggesting that multiple growth factors evoked the upregulation of FLK1 and VEGFR2 expressions over the single factor (ie, VEGF), thereby possibly amplifying VEGF release. The understanding of our results may be translated into the emerging concept that SMCs support the biological aspects of EPCs via the endothelial–pericyte cytokine cross-communication.

The mechanism of restoration of damaged myocardium by EPC transplantation is complex.[2,3,13] Although cytokine release and hematopoietic stem cell recruitment have been proposed as possible mechanisms of regeneration, other important mechanisms are likely to be involved. The creation of mature, stable, and functional vessels is essential. It has been reported

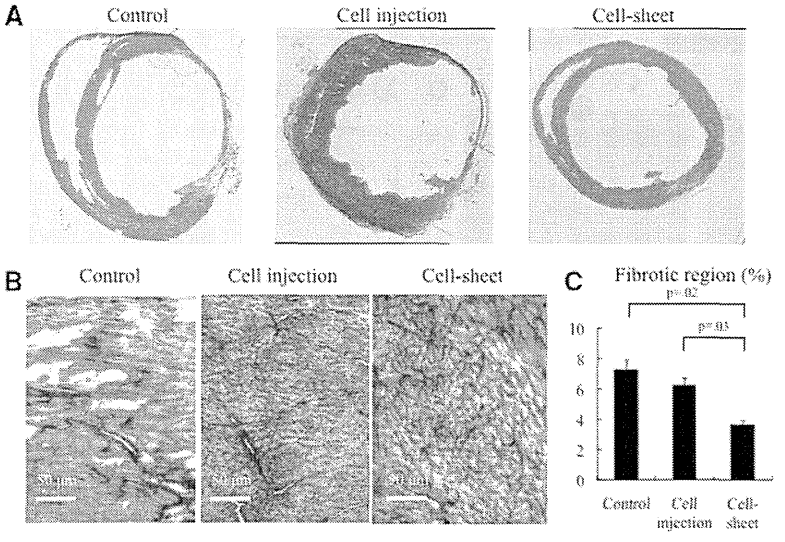


**Figure 5. A**, Representative macroscopic views of the heart (hematoxylin-eosin staining). The myocardial structure was superiorly maintained after cell-sheet transplantation compared with cell injection and control. **B**, Representative Masson trichrome staining at the borderzone myocardium. **C**, Quantification of fibrotic region. Fibrosis at the borderzone area was significantly suppressed in the cell-sheet group compared with the other groups (cell sheet, n=4; cell injection, n=3; control, n=4; *P*=0.02, Kruskal–Wallis test).

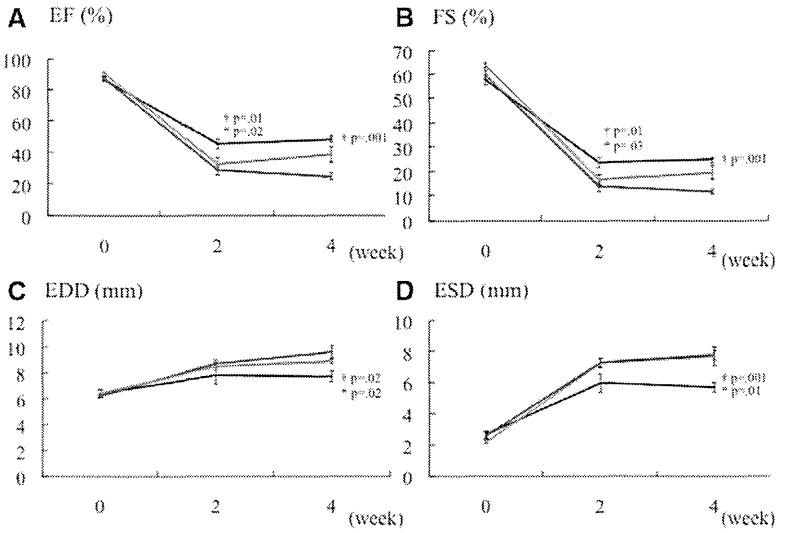


**Figure 6.** Serial changes in (**A**) ejection fraction (EF), (**B**) fractional shortening (FS), (**C**) end-diastolic diameter (EDD), and (**D**) end-systolic diameter (ESD) assessed by echocardiography (cell sheet, n=7, black line; cell injection, n=8, red line; control, n=9, blue line). Examinations were performed before (0) and at 2 and 4 weeks of follow-up after the operation. EF and FS were significantly higher at 2 and 4 weeks in the cell-sheet group compared with either cell injection or control (EF at 2 weeks, *P*=0.01; EF at 4 weeks, *P*=0.003; FS at 2 weeks, *P*=0.01; FS at 4 weeks, *P*=0.003; Kruskal–Wallis test). EDD and ESD were lowest at 4 weeks in the cell-sheet group (EDD, *P*=0.02; ESD, *P*=0.003; Kruskal–Wallis test). **P*<0.05 vs cell injection; †*P*<0.05 vs control, post hoc pairwise Wilcoxon–Mann–Whitney *U* test.

that capillary formation occurs via two basic vessel-constructing processes: angiogenesis (ie, the formation of new capillaries via sprouting or intussusception from preexisting vessels) and vasculogenesis (ie, de novo formation of vasculature as occurs in the developing embryo).[21] It has also been reported that angiogenesis requires a dynamic temporally and spatially regulated interaction among endothelial cells, pericytes, and angiogenic factors.[22] Given the natural relationship between endothelium and intima within mature vessels, we added SMCs, which are essentially vascular pericytes, to enhance the angiogenic performance of EPCs. Thus, it was hypothesized that coculturing EPCs with SMCs would promote a robust angiogenic response and induce formation of mature blood vessels. Our present study shows that in addition to the

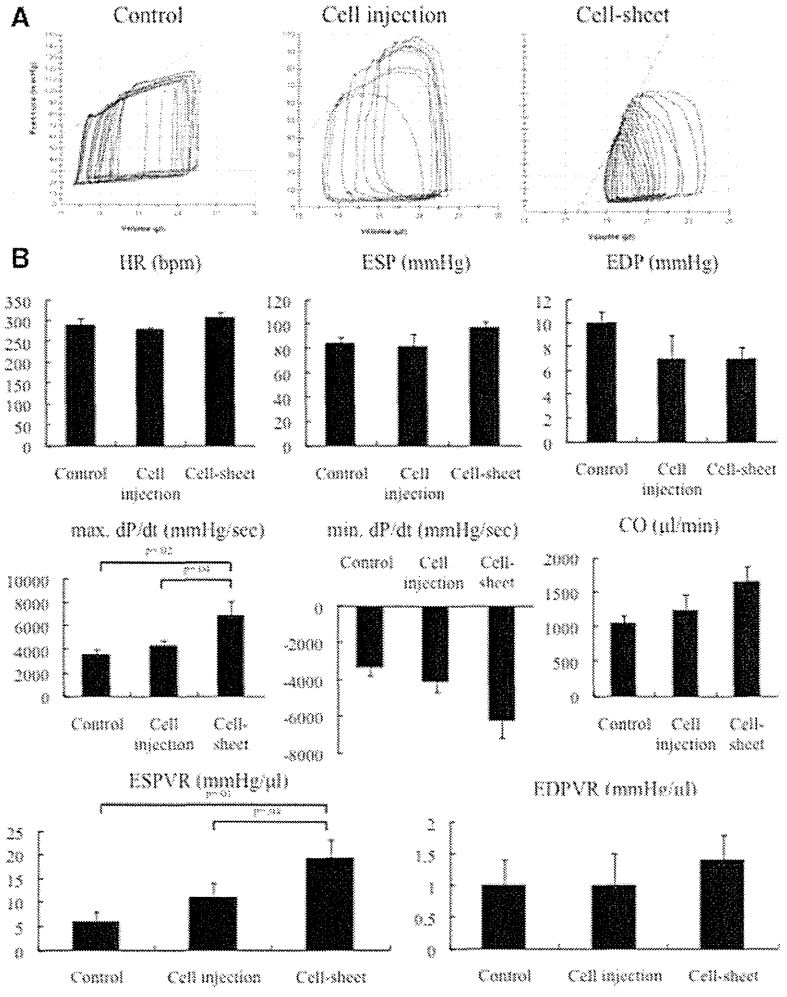


**Figure 7.** Hemodynamic measurements determined using cardiac catheterization after cocultured bi-level cell-sheet transplantation (cell-sheet, n=6), cocultured cell injection (cell injection, n=6), and control (control, n=8). Examinations were performed at 4 weeks of follow-up after the operation. **A**, Representative pressure–volume loops during inferior vena cava occlusion from cell-sheet, cell injection, and control groups. **B**, There was no significant difference in heart rate (HR), end-systolic pressure (ESP), end-diastolic pressure (EDP), mimimal rate of change in left ventricular (LV) pressure (min. d*P*/d*t*), cardiac output (CO), or end-diastolic pressure–volume relationship (EDPVR; HR, *P*=0.35; ESP, *P*=0.19; EDP, *P*=0.14; min. d*P*/d*t*, *P*=0.05; CO, *P*=0.07; EDPVR, *P*=0.70; Kruskal–Wallis test). The maximal rate of change in LV pressure (max. d*P*/d*t*) and end-systolic pressure–volume relationship (ESPVR) significantly improved in the cell-sheet group compared with the other 2 groups (max. d*P*/d*t*, *P*=0.04; ESPVR, *P*=0.03; Kruskal–Wallis test).